2019-08-09

Optimizing CRISPR/Cas9 for Gene Silencing of SOD1 in Mouse Models of ALS

Zachary C. Kennedy
University of Massachusetts Medical School

Optimizing CRISPR/Cas9 for gene silencing of SOD1 in mouse models of ALS

A Dissertation Presented

By

ZACHARY C KENNEDY

Submitted to the Faculty of the University of Massachusetts Graduate School of Biomedical Sciences, Worcester

In partial fulfillment of the requirements for the degree of

DOCTOR OF PHILOSOPHY

09 August 2019

Neuroscience Program

Optimizing CRISPR/Cas9 for gene silencing of SOD1 in mouse models of ALS

A Dissertation Proposal

BY

Zachary C Kennedy

This work was undertaken in the Graduate School of Biomedical Sciences

Neuroscience Program

Under the mentorship of

Robert H Brown Jr, MD-DPhil, Thesis co-advisor

Wen Xue, Ph.D., Thesis co-advisor

&

Daryl Bosco, Ph.D., Member of Committee

Lawrence Haywood, MD, PhD, Member of Committee

Diane Lipscombe, PhD, External Member of Committee

Erik Sontheimer, Ph.D., Chair of Committee

Mary Ellen Lane, Ph.D.,

Dean of the Graduate School of Biomedical Sciences

Dedication

I would like to dedicate this thesis to my wife, Samantha Kennedy who loved and supported me throughout my entire scientific career.

I would also like to dedicate this thesis in the memory of Peter Sapp, who trained me in my first job as a scientist. Your presence in the lab and your beermaking skills continue to be missed.

Acknowledgements

I would like to thank Dr. Wen Xue for accepting me into his lab and allowing me to collaborate with the Brown lab. Sharing a student has its own unique challenges, and we both navigated these challenges together. He gave me the freedom to pursue the project I wanted, all while giving me guidance, support, and endless varieties of CRISPR plasmids. He taught me about how to design and test CRISPR-based strategies for translational projects.

I am grateful for my Thesis Advisory Research Committee (TRAC) chair Erik Sontheimer, and my TRAC members, Daryl Bosco, Lawrence Hayward and Chris Mueller. All members have been engaged, passionate and helpful; It was a pleasure (albeit a nervous pleasure) to have the opportunities to present my work and discuss the findings with these people.

I would also like to thank Diane Lipscombe, who along with the TRAC committee members, comprise my dissertation examination committee. Diane posed helpful questions and provided even more helpful insight to my thesis.

I am immensely thankful for all members of the Xue lab who have helped me along the way. I thank Haiwei Mou, Soren Hough, Angela Park, Suetyan Kwan, Chunqing Song, Tingting Jiang, Jordan Smith, Ankus Sheel and Simon Liang. All of them have been there for me, from providing troubleshooting, engaging me in scientific discussions, providing tremendous support when

experiments have failed, and sharing with me Wegman's brand cheeseball puffs. Haiwei, I specifically thank you for scientific insight and your philosophy, you have taught much on life as you did science. Suetyan, I specifically thank you for training me in cell-culture and lentiviral work, and I apologize for the liters of cell-culture media I 'borrowed' from you.

I thank Dr. Bob Brown for enthusiastically supporting my project from the very beginning. Dr. Brown's limitless enthusiasm and tenacity in his pursuit of develop treatments for ALS is truly a privilege to witness. From the very beginning, Dr Brown acted above and beyond the norm to support my scientific training. From meeting me at weird hours to review data, connecting me to colleagues within the ALS world, and reviewing my presentation before conferences, thank you. I will echo the toast you gave at my thesis dissertation; "To a cure".

I thank everyone in Dr. Brown's lab who have helped me throughout the years; Peter, Nick, Owen, Gaina, Alex, Jake, Ozgun, Justin, Sena, Janice, Siqi, Gloria, Huiya, Hezhang, Harry, Karla, Cecile, Cat Douthwright, Hirosha, Nils, Diane, Julia, Kat Mocarski, Peter, Karen, Helene, and Franck. Special thanks to Alex and Jake for the hours of time they spent training me on how to handle mice.

I would like my Mom and Dad for three decades of thankless and tiresome work, preparing me to tackle challenges both professionally and personally. I am

grateful now, and I am honored and blessed to have grown up with you. Truly humbled to be considered as one of your top 4 best children.

I would like to thank the Angel Fund and their fundraising efforts because I could not have done this work without their financial support.

Abstract

Mutations in the *SOD1* gene are the best characterized genetic cause of amyotrophic lateral sclerosis (ALS) and account for ~20% of inherited cases and 1-3% of sporadic cases. The gene-editing tool Cas9 can silence mutant genes that cause disease, but effective delivery of CRISPR-Cas9 to the central nervous system (CNS) remains challenging. Here, I developed strategies using canonical *Streptococcus pyogenes* Cas9 to silence *SOD1*. In the first strategy, I demonstrate effectiveness of systemic delivery of guide RNA targeting *SOD1* to the CNS in a transgenic mouse model expressing human mutant SOD1 and Cas9. Silencing was observed in both the brain and the spinal cord. In the second strategy, I demonstrate the effectiveness of delivering both guide RNA and Cas9 via two AAVs into the ventricles of the brain of *SOD1*^{G93A} mice. Silencing was observed in the brain and in motor neurons within the spinal cord. For both strategies, treated mice had prolonged survival when compared to controls. Treated mice also had improvements in grip strength and rotarod function. For ICV treated mice, we detected a benefit of SOD1 silencing using net axonal transport assays, a novel method to detect motor neuron function in mice before onset of motor symptoms. These studies demonstrate that Cas9-mediated genome editing can mediate disease gene silencing in motor neurons

and warrants further development for use as a therapeutic intervention for *SOD1*-linked ALS patients.

Table of Contents

List of Tables

List of Figures

Copyright Materials Produced by Author

Preface

Data presented in this dissertation are the result of two projects that I conceived, designed and executed under the guidance of Dr. Robert Brown and Dr. Wen Xue. Data from the project titled “CNS delivery via ICV injection of Cas9 and guide RNA targeting *SOD1* prolongs survival” has been submitted for publication as part of a manuscript co-authored by myself and Pin-Tsun “Justin” Lee. Detailed contributions can be found in the specific chapter prefaces. Chapters I and III are unpublished original work of mine that I wrote for this dissertation.

Chapter I Introduction

1.1 Amyotrophic Lateral Sclerosis

Amyotrophic lateral sclerosis (ALS), commonly referred to as Lou Gehrig's disease (United States) and Motor Neuron Disease (United Kingdom), is an adult-onset neuromuscular degenerative syndrome characterized by motor neuron degradation and progressive paralysis. ALS affects both upper and lower motor neurons (Fig. 1), which distinguishes this disease from other motor-neuron disorders (i.e., primary lateral sclerosis, progressive supranuclear palsy, and corticobasal syndrome). ALS is uniformly fatal; death typically occurs 3-5 years after onset.[2]

First described by the French neurologist Jean-Martin Charcot in 1874, ALS is the most common adult-onset motor neuron disease in the U.S.— the annual incidence of ALS is 400,000 people per year. Worldwide, ALS prevalence is approximately 6 per 100,000 people, and the incidence is approximately 2 per 100,000 annually[3,4]. This equals approximately 140,000 new cases every year or 384 new cases per day worldwide. Incidence changes with age, increasing after age 50, but rapidly decreasing after age 80. Incidence is also higher among men than women: 3 and 2.4 per 100,000, respectively[4].

.

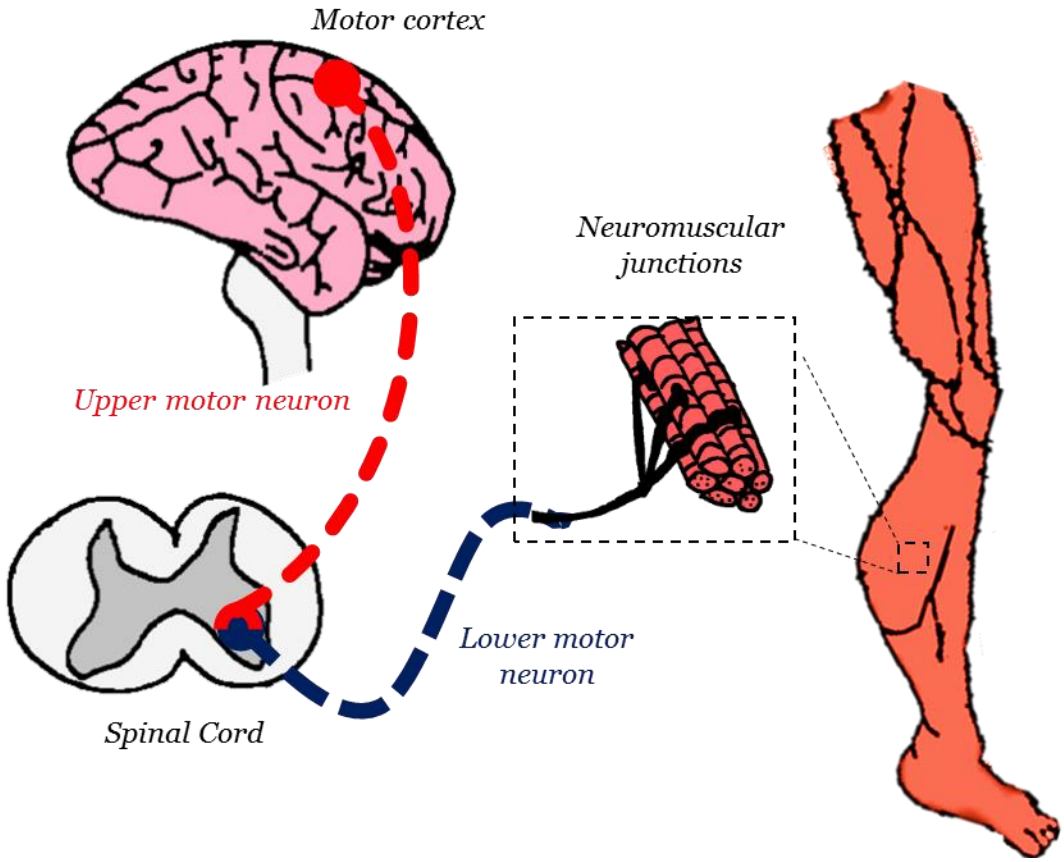

Figure 1. Anatomy of motor neurons affected by ALS.

Upper motor neurons reside in the motor cortex and their axons project down the spinal cord through the corticospinal tracts project and innervate lower motor neurons the axons. Cell bodies of lower motor neurons reside in the ventral horn of the spinal cord and project through the ventral root to innervate muscles. Neuromuscular junctions are the points of connection between lower motor neurons and muscles.

Additionally, ALS is now widely considered to be part of a spectrum of neurological disorders that include ALS-frontotemporal lobar degeneration (FTLD). FTLD is the fourth most common adult onset neurodegenerative

disorder, behind Alzheimer's, Parkinson's, and ALS. The connection between ALS and FTLD was recognized as early as 1932[5]. Many patients present with symptoms of both disorders[6,7], and patients diagnosed with either ALS or FTLD often develop symptoms of the other. These disorders have overlapping biochemical hallmarks (FUS and TDP43 protein aggregation), and overlapping gene mutations, which include *C9ORF72, HNRNPA1, HNRNPA2B2, SIGMAR1, ATXN2, SQSTM1, OPTN, VCP, UBQLN2* and *CHCHD10*. Thus, developing treatments for ALS could potentially be beneficial for FTLS cases as well. There is, however, no cure for either disorder

Currently, there are two FDA-approved drugs for ALS aimed at slowing disease progression. Each drug provides only modest benefits. Riluzole, a sodium channel blocker approved in 1995, may extend patient survival by 2-3 months[8]. Edaravone, a novel free-radical scavenger approved in 2017, slowed early-stage ALS progression in a 6-month trial[9,10]. However, the impact of edaravone on patient survival has yet to be reported. Recently new interventions have progressed into clinical trials.

The causes of approximately 90% of ALS cases are unknown or "sporadic", but 10% of cases are genetically inherited or "familial". To date, over 30 genes are robustly associated with familial ALS. Among these genes, the free-radical scavenger—copper-zinc superoxide dismutase 1 (*SOD1*)—was the first to be linked to ALS[11]. Over 100 different *SOD1* mutations are ALS-related[12].

ALS treatment strategies intending to silence or knockdown the *SOD1* gene are appealing because: **(1)***SOD1* mutations associated with ALS have a gain-of-function toxicity; **(2)** *SOD1* mutations are common, accounting for ~20% of familial cases and in 1-3% of sporadic cases[13–16]; **(3)** Among ALS mutations, those in *SOD1* are the best characterized—numerous *SOD1* animal models recapitulate hallmark features of ALS, including adult onset neurodegeneration and paralysis[17], making it feasible and tractable to study gene silencing strategies; and **(4)** Patients with wildtype *SOD1* (wt*SOD1*) often have SOD1 aggregation similar to that observed in patients with mutant SOD1, which may suggest that both mutant and wtSOD1 contribute similarly to disease pathology[15], and therapeutic *SOD1* gene silencing might benefit patients with or without mutant SOD1. Effect design of such silencing strategies, however, require an in-depth understanding of SOD1, and how mutations change the characteristics of the protein and how these changes cause or progress symptoms in ALS.

1.2 SOD1 and ALS

The protein product of the SOD1 gene dismutates superoxide free radicals into molecular oxygen and hydrogen peroxide[13]. SOD1 protein resides primarily in the cytoplasm, but also localizes to mitochondria; it is highly expressed, comprising ~1-2% of total protein in cultured cells[18]. SOD1 is a member of the superoxide dismutase family.

The catalytically-active, holoenzyme form of SOD1 is a homodimer that weighs ~32 kilodaltons. Notable structural features of SOD1 include an eight-stranded β-barrel structure, a zinc-binding loop, an electrostatic loop, and a cysteine-cysteine disulfide bond, a rare characteristic for proteins residing in the cytosol. Each subunit binds one copper and one zinc ion, both of which contribute to structural stability[19,13,16,20]. Homodimerized SOD1 is highly stable; it has a melting temperature (T_m) of 92ºC, much higher than physiological conditions, and is resistant to both chaotropic and ionic denaturization[7,12]. SOD1 is also one of the fastest enzymes known; its rate-limiting step is the diffusion of superoxide to its active site[21]. It is the positively-charged electrostatic loop of the enzyme that brings the negatively-charged superoxide towards the active site, where both copper and zinc contribute to dismutation[22].

ALS-associated *SOD1* mutations generally have two common features: (1) destabilization of the protein, causing aberrant misfolding/aggregation; and (2) reduced dismutase activity, causing oxidative stress[16,20]. While these two features certainly contribute to toxicity, how they initiate ALS remains unknown. Numerous candidate pathways have been investigated, including synaptic dysregulation/excitotoxicity, mitochondrial dysfunction, and impairment of autophagy/proteasome[15,20,23] (Fig. 2). However, more work is required to dissect which of these interwoven pathways cause ALS, and which are merely consequences of upstream stressors. Such findings are critical for the design of drug therapies. The subsequent subchapters briefly review oxidative stress,

protein misfolding/aggregation, and the putative downstream pathways affected by oxidative stress/protein misfolding and the evidence of their role in ALS.

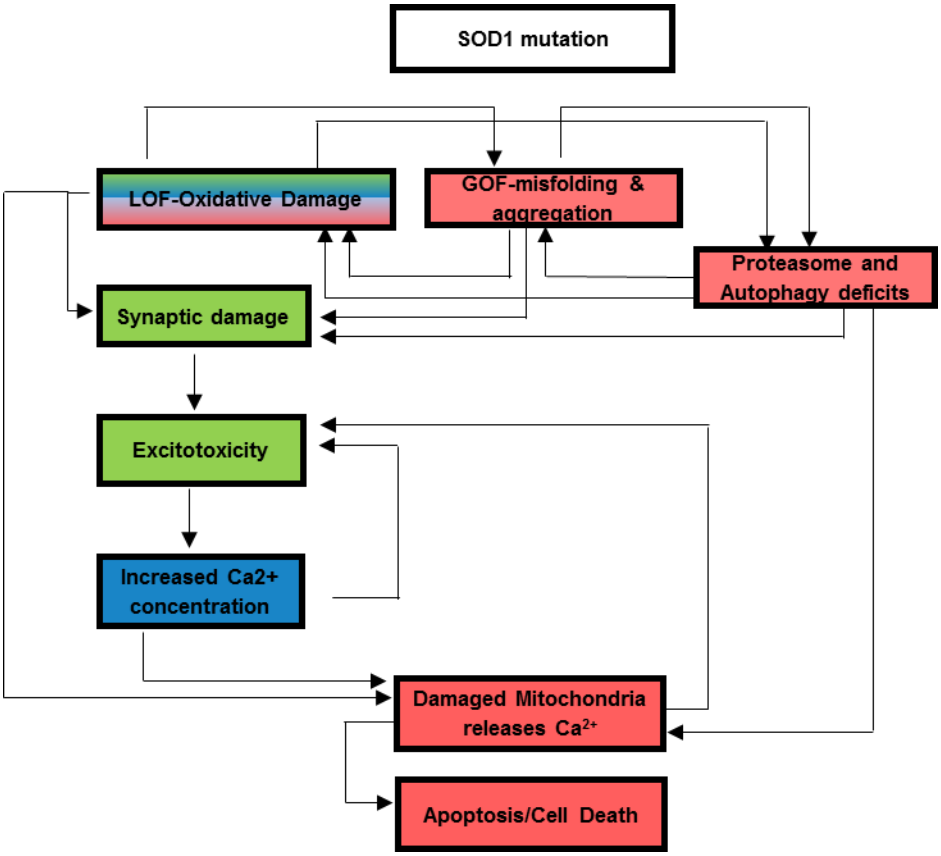

Figure 2. Neuronal pathways of damage in *SOD1* ALS

Proposed chain of events that leads to motor neuron degeneration in SOD1 ALS. Oxidative stress and/or SOD1 misfolding/aggregation are likely upstream events that trigger dysregulation of the synapse, proteasome, autophagy, and mitochondria. Dysregulation of these processes causes increase in Ca^{2+} which in turn can trigger apoptosis. Red indicates process which occurs in the cell body. Blue indicates process which occurs in the synaptic membrane. Green indicates process indicates process which occurs in axon/post synaptic membrane. Gradient indicates process occurs in cell body, synaptic membrane and axon.

1.2.1 SOD1 and Oxidative Stress

The first genetic mechanism hypothesized to cause ALS was SOD1 haploinsufficiency followed by oxidative stress. This mechanism was proposed shortly after the discovery of ALS-associated *SOD1* mutations when evidence of reduced SOD1 activity and oxidative stress was found in ALS patient brains[24,25,27,28]. Additionally, biochemical analyses demonstrate that many ALS-associated *SOD1* mutations result in diminished or complete loss of dismutation activity *in vitro*[26].

SOD1 loss of function, however, cannot fully explain SOD1-linked ALS pathogenesis because: (i) there is a lack of correlation between mutant SOD1 dismutase activities and clinical outcome (i.e., a patient with a *SOD1* mutation that causes 50% dismutase activity does not have a worse clinical outcome than a patient with an *SOD1* mutation that causes 0% activity), (ii) no ALS-like phenotype is observed in *Sod1*-null mice (although *Sod1*-null mice do have mild denervation and neuropathy[27]), and (iii) transgenic mouse models of ALS, which robustly phenocopy neurodegeneration, have increased net dismutase activity due to the multiple copies of transgenes inserted[27–29]. These observations lead to the investigation of other potential mechanisms of ALS pathology.

1.2.2 SOD1 misfolding and aggregation

Mutant SOD1 and wtSOD1 have been shown to misfold and aggregate *in vitro, in vivo*, and in ALS patients[13,30]. Mutations in *SOD1* result in altered monomer-dimer homeostasis, favoring the monomer state. Monomer-dimer homeostasis can also be disrupted in wtSOD1 under certain stressors like demetallation and reduction of the C57–C146 intramolecular disulfide bond. In both cases, monomeric SOD1 is more likely to oligomerize into soluble aberrant conformations and aggregate into insoluble fibrils, a pathological hallmark of *SOD1* ALS.

Evidence of mutant SOD1 aggregation first came in 1994, when Lewy body-like inclusions in spinal cords of sporadic ALS patients were found to be immunoreactive to SOD1[30]. Mutant SOD1 was also reported to cause abnormal aggregations in cultured neurons[31] and in transgenic *SOD1* mice[16]. Multiple lines of evidence demonstrate that SOD1 misfolding and aggregation is toxic. SOD1 aggregations cause cell death in cell culture and can spread to neighboring cells in a “prion-like” fashion[32,33]. Moreover, SOD1 aggregate levels in the CNS increase and correlate with disease progression in ALS mouse models[34,35]. Distinct from ‘aggresomes’, mutant SOD1 oligomers have also been observed in transgenic mice[36]. Interestingly, recent evidence suggests that the soluble oligomeric conformations of SOD1 are toxic while the insoluble aggregates may be sequestered by the cell and rendered inert[37].

While mutant forms of SOD1 are more prone to misfolding, even misfolded wtSOD1 can be detected in sporadic ALS patients, suggesting an

association between SOD1 misfolding and ALS, although the mechanisms driving the disease initiation and progression remain unclear [38,15,30].

While evidence supports SOD1 misfolding toxicity, it is still unclear how it causes ALS. The current hypothesis is that the synergism of oxidative stress and SOD1 misfolding contributes to ALS. Specifically, SOD1 aggregation causes a 'gain of a loss of function', where a toxic gain-of-function from misfolding exacerbates oxidative damage that cannot be mitigated due to SOD1 reduction of function[28,39,40]. Pathways known to be dysregulated in ALS that are affected by SOD1 misfolding include: (1) synaptic dysregulation/excitotoxicity, (2) mitochondrial dysfunction, and (3) autophagy/proteasome impairment.

1.2.3 SOD1 and synaptic dysregulation/excitotoxicity

One of the first symptoms of ALS, preceding even muscle weakness, is fasciculation (or muscle twitching) caused by distal axon dysfunction. Aberrant upper and lower motor neuron electrical signaling—i.e. synaptic dysregulation—in ALS was first demonstrated in electrophysiological studies of patients [41,42]. In 1995, biochemical evidence for synaptic dysregulation came when altered glutamate levels in post-mortem tissue and CSF were described in a subset of ALS patients[43,44]. Glutamate, the major excitatory neurotransmitter found in mammalian excitatory synapses, is an agonist for ionotropic transmembrane receptors, including those found in motor neuron synapses: α-3-amino-3

hydroxy-5-methyl-4-isozaxelopropionic (AMPA) and N-methyl-D-aspartic acid (NMDA).

SOD1 mutations may cause ALS via glutamate dysregulation and consequent synaptic dysregulation. It is thought that in ALS, a feedback loop emerges where oxidative stress causes more oxidative stress. In humans, the main protein responsible for shuttling glutamate out of the synapse, Excitatory Amino Acid Transport 2 (EAAT2), is reduced in some ALS patients [32,33,45–47], leading to increased and persistent glutamate concentrations in motor neuron synapses [48,49]. Elevated glutamate concentrations in the synapse causes hyperactivity, or pathologic increase of action potential firing in the post-synaptic neuron[50]. Hyperactivity also increases intracellular Ca^{2+} levels—which in turn activates the stress signals nitric oxide synthase, phospholipase A2, and xanthine oxidase[49], which in turn increases oxidation and can cause further perturbations to glutamate homeostasis. This oxidative damage feedback mechanism may help explain why ALS causes degeneration specifically in motor neurons, as spinal motor neurons have inherently weak Ca^{2+} buffering capacity [48,50,51], thus making them sensitive to excitotoxic insults.

Glutamate dysregulation, however, cannot fully explain pathogenesis because reduced brain and CSF glutamate is observed in only a subset of patients. Furthermore, EAAT2 downregulation occurs in other neurological conditions, such as Alzheimer's, ischemic hypoxia, and traumatic brain injury, suggesting that it may be a generalized consequence of damage.

1.2.4 SOD1 and mitochondria dysfunction

Mitochondrial dysregulation in ALS was observed as early as 1984 in electron microscopy studies. Mitochondria in skeletal muscle and spinal cord neurons of ALS patients have abnormal morphologies[52,53], including vacuolization, swollen cristae, and perturbations to the inner and outer membranes. Functional deficits of mitochondria in ALS include defects in electron transport protein complex activity and Ca^{2+} buffering capacity. Given that both electron transport protein complex disruption and Ca^{2+} defects cause the release of proapoptotic factors[54–56], it is proposed that mitochondrial perturbation initiates apoptosis. Recent findings that mutant SOD1 binds to apoptosis regulator gene BCL2, which can promote apoptosis under certain conditions, supports the notion that mitochondrial dysregulation drives toxicity via apoptotic pathways[57–59].

Mitochondrial abnormalities are also seen in Alzheimer's, Parkinson's and Huntington's suggesting that they may be a generalized consequence of unspecified damage, and not a cause of ALS. Indeed, oxidative stress causes mitochondrial stress, but mitochondrial defects precede ALS symptoms in the *SOD1*^{G93A} mouse model. This suggests that mitochondrial damage may be the pathogenic factor, not a downstream consequence.

1.2.5 SOD1 and impairment of autophagy and proteasome

The proteasome and autophagy pathways regulate protein homeostasis and eliminate toxic protein species in eukaryotic cells. Recent evidence shows that mutant SOD1 is degraded by and impairs both proteasome and autophagy processes[60].

Proteasome. The proteasome is a large, multi-subunit complex that degrades proteins by breaking peptide bonds through multiple catalytic sites. Proteins are polyubiquitinated by E3 ubiquitin ligases, marking them for degradation. Misfolded forms of mutant SOD1, but not wtSOD1, are polyubiquitinated for proteasome degradation and cause proteasomal inhibition in neuronal cell lines[59]. Immunoprecipitation studies by multiple groups revealed that mutant SOD1 is specifically targeted by the ubiquitin ligases Dorfin, CHIP, NEDL1, and the mitochondrial-expressing MITOL[61–63]. Interestingly, two of these ubiquitin ligases have previously described roles in neurodegeneration—Dorfin activity is involved in Lewy body aggregation in Parkinson's Disease[64], and mutations in CHIP cause Spinocerebellar ataxia type 16[62,65].

Not only is mutant SOD1 targeted by the proteasome, but mutant SOD1 impairs proteasome function. Overexpression of Dorfin in the presence of mutant SOD1 in neuronal cell culture reduces cell death, suggesting that mutant SOD1 impairs the proteasome in ALS[64]. This is supported by recent evidence of proteasome dysregulation in patients, with increased levels of ubiquitin and

proteasomal αβ subunits found in spinal cords of end-stage ALS patients compared to healthy controls[66].

A SOD1 proteasome model for toxicity in ALS has been proposed: prior to disease onset, misfolded SOD1 is cleared by the proteasome and protein homeostasis is maintained. A combination of excessive misfolded protein and oxidative stress due to SOD1 dysregulation overwhelms the proteasome causing a feedback loop of increased SOD1 misfolding and proteasome dysregulation.

Autophagy. Autophagy is the regulatory process in which a cell sequesters components into membrane-bound vesicles called autophagosomes, and fuses with hydrolytic-enzyme-containing lysosomes to degrade the contents. Autophagy levels are tightly linked to cell survival, either promoting survival by clearing damaged organelles, proteins, and toxic metabolites or mediating cell death through self-digestion[67].

In *SOD1*^{G93A} mice, increased levels of autophagy vacuoles have been found in late stages of disease[68], although this may be a consequence of upstream toxicity. In addition, many mutant SOD1 binding partners have roles in regulation autophagy: 1) BCL2, which inhibits autophagy via binding of autophagy formation protein, Beclin1; and 2) P62, which is involved in autophagy activation[67,69]. Interestingly, *P62* gene mutations cause a subset of familial ALS[70].

A drug screen revealed that inhibitors of the mTOR pathway, which regulates autophagy, increased survival percentage of cultured neurons and

SOD1 mouse models of ALS[71] by 8 days, suggesting that autophagy impairment plays a role in SOD1 toxicity.

1.3 Suppressing SOD1 as a therapeutic strategy

Despite the ambiguity of how mutant SOD1 initiates and drives ALS, genetic silencing of *SOD1* has proven to be a rational and viable strategy for therapy of *SOD1* mediated ALS. Silencing *SOD1* ameliorates neurodegeneration by delaying onset, and increasing survival in *SOD1* animal models[14,23,72–74]. Interestingly, since aberrant SOD1 misfolding is also observed in a subset of ALS patients who do not have a *SOD1* mutation, it is conceivable that silencing *SOD1* may be of therapeutic benefit to a subset of sporadic ALS patients that do not have mutant *SOD1*. Regardless, the wealth of literature describing the outcomes of *SOD1* silencing has allowed for analysis of the mouse model; an excellent candidate for studying the therapeutic potential of CRISPR-based gene editing.

Previous strategies used to repress *SOD1* in transgenic animal models include neutralizing antibodies[34], antisense oligonucleotides (ASOs)[75], short hairpin RNA (shRNA)[73,76,77], artificial microRNA (miR)[72], and chemically-modified shRNA[23] (Table 1). The wealth of knowledge gained from previous experiments allows for the design, development and optimization of new *SOD1* silencing strategies that may be more efficacious for therapy, such as increased survival,

and reduced number of injections. Outlined below are key concepts that have been elucidated in previous *SOD1* silencing research.

Vector	Construct	Delivery	Treatment start	Animal	Survival (%)	1st Author	Year
Lentivirus	shRNA	IM	p7	Mouse	77	Ralph	2005
Lentivirus	shRNA	IS	p40	Mouse	nr	Raule	2005
Transgene	shRNA	systemic	embryonic	Mouse	27	Xia	2006
-	ASO	ICV	p65	Rat	8	Smith	2006
Mod. siRNA	siRNA	IT	p85	Mouse	6	Wang	2008
AV-U6	shRNA	SN	p94	Mouse	8	Wu	2009
AAV2	shRNA	SN	p43-109	Mouse	0	Wu	2009
--	monoclonal ab	ICV pump	p65	mouse	8	Gros-Louis	2010
AAV6	shRNA	IM	p1-p15	Mouse	0	Towne	2011
AAV9	shRNA	IV	p1	Mouse	39	Foust	2013
--	ASO	IT	post disease onset	human	-	Miller	2013
AAVrh10	miR	IT	p55-60	Mouse	11	Wang	2014
--	single chain ab	IT	p45	mouse	11	Patel	2014
AAV9	shRNA	IC	p70	Rat	12	Thompsen	2015
AAV6	miR	ICV	p2	Mouse	26	Dirren	2015
AAV9	miR	ICV	p2	Mouse	14	Dirren	2015
AAVrh10	miR	IV	p56-68	Mouse	20	Borel	2016
AAV9	miR	ICV	p0-1	Mouse	50	Stoica	2016
AAV9	Cas9	IV	p1	mouse	25	Gaj	2017

Table 1. *In vivo* silencing of *SOD1*

(IM) Intramuscular. (IV) Intravenous. (SN) Sciatic Nerve. (ICV) Intracerebroventricular. (IT) Intrathecal. (IC) Intracortical. (miR) microRNA.

Allelic targeting of SOD1. Most silencing experiments have, out of practicality, targeted both mutant and wt. alleles because transgenic mouse models contain only the mutant human allele. Initially, this raised concerns about potential detrimental effects, but concerns subsided somewhat because silencing wt*SOD1* appears to be tolerable in the CNS[78]. Indeed, experiments that silenced both human *SOD1* and mouse *Sod1*, comparable to a biallelic *Sod1*-targeting strategy in patients, prolonged survival without overt adverse symptoms[78]. Furthermore, *Sod1*-null mice have no overt motor degenerative phenotype or motor neuron loss, although there is enhanced cell death after axonal injury, 30% shortening of life span and higher incidence for hepatocellular carcinoma[27,79].

Timing of Intervention. In mouse models, *SOD1* silencing at early timepoints is more beneficial than later timepoints. Experiments by Foust *et al*. show that delivering adeno-associated viral vectors (AAVs) containing shRNA via facial vein delivery at p1-2 had a maximum prolongation of survival, and survival benefits decreased with increasing age at delivery[73]. Despite the benefit of early intervention, Foust *et al*. showed the delivery of shRNA as late as p85 could significantly prolong survival, suggesting silencing of *SOD1* could prove useful in the clinic.

Similarly, experiments by Borel *et al.* using AAVs delivering artificial microRNA via intracerebroventricular delivery at day 56-58 prolonged survival[14], and experiments by Gros-Louis *et al.* showed that silencing of *SOD1* by using monoclonal antibodies against SOD1 at p65 could extend survival[34]. These

studies demonstrate that *SOD1* silencing in patients could be beneficial when given to adults prior to disease onset. More research is needed to understand the effects of *SOD1* silencing in patients after onset.

In most cases, silencing delays onset, but does not prevent or reverse neurodegeneration, or duration of disease (*i.e.*, the time between disease onsets and endpoint remains the same). However, there are some notable exceptions.

Saito *et al*, reported an increase in duration of disease in a *SOD1*^{G93A} - mouse model. However, in Saito's experimental paradigm, mutant *SOD1* was targeted at conception via crossing *SOD1* mice with mice expressing shRNA[78]. Borel *et al.* reported that delivering artificial microRNA prolonged disease duration when the expression of the microRNA was under a pol II Chicken Beta actin promoter but not a pol III-type U6 promoter[14]. It is unclear why the promoter caused differences in disease duration.

Stoica *et al.*, also reported a subset of mice that did not undergo normal neurodegeneration: rather, the mice treated at day p1 showed little degeneration as measured by electrophysiology and died following sudden weight loss and kyphosis[14]. In the subset of mice, disease duration was eliminated because the mice did not undergo canonical degeneration.

Cell type-specific SOD1 targeting. Motor neurons are primarily affected by ALS, but numerous studies have shown that such toxicity is not solely cell-autonomous. Microglia[80], astrocytes[81], oligodendrocytes[82] and skeletal muscle [83] contribute to SOD1-mediated motor neuron toxicity. The research to-date shows

that silencing *SOD1* specifically in astrocytes[84] leads to a benefit in survival, while silencing *SOD1* in muscle only does not translate to increased survival[85–87]. More research is needed to understand whether silencing *SOD1* in other cell types leads to increased survival.

Previous experiments have focused on *SOD1* silencing in lower motor neurons, which reside in the spinal cord. There is comparatively less literature discussing the state of neurodegeneration in upper motor neurons in transgenic mouse models. Özdinler *et al*. demonstrated that upper motor neurons undergo specific neurodegeneration as early as p30[88], which recapitulates what occurs in ALS patients. Moreover, Thomsen *et al*. demonstrated that silencing *SOD1* in the motor cortex, and not the spinal cord, leads to a 20-day extension in survival in *SOD1* rats[74].

The collective observations from previous work provides a framework for developing strategies to silence *SOD1*. Such strategies should focus on early intervention, non-cell type specificity, and targeting of both upper and lower motor neurons.

1.4 Therapeutic *SOD1* silencing using CRISPR-Cas9

CRISPR-Cas9 mediated gene therapy has emerged as a potent gene editing technology. It is an easy-to-use, cost-effective tool that targets and cleaves desired regions of genome DNA allowing for the silencing and/or repair

of mutant gene expression. CRISPR-Cas9 technology was engineered from bacterial/Archaea CRISPR systems which provide sequence-specific, adaptive immunity to invading nucleic acids like viruses and mobile elements.

As bacterial/archaeal immune components, CRISPR systems work by integrating short sequences of invading DNA (e.g., bacteriophages, virions, and mobile DNA elements) into the CRISPR gene locus, creating a memory of infection. In subsequent invading DNA infections, the previously inserted DNA is transcribed into a short strand of RNA called crRNA and forms an effector complex with CRISPR associated (Cas) proteins and yet another strand of RNA called tracrRNA. This effector complex cleaves the invading DNA, mitigating harmful effects of the infection.

CRISPR systems are broadly found in bacteria/archaea and have been identified in the genomes of approximately 40% of sequenced bacteria and 90% archaea [89]. CRISPR systems are very diverse in terms of the structure of the CRISPR locus, the composition of proteins, and the structure of the effector complex. Classification of CRISPR systems currently divide CRISPR systems into 2 Classes (Class 1 and Class 2), and subdivided into 6 types (Type I through Type VI)[90]. Class 1 CRISPR systems are defined as having multiple protein subunits in their effector complex while Class 2 CRISPR systems are defined by having a single protein, called Cas9, in the effector complex. Two major events made it possible to develop CRISPR-Cas9 into a gene-editing technology: (1), the discovery that Cas9 enzymes could be reprogrammed to target a desired

DNA sequence[91] and (2), the engineering of a single strand of RNA that functions as both crRNA and tracrRNA, thus simplifying both designing and manufacturing of CRISPR-Cas9 based gene editing strategies[92,93].

The steps by which Cas9 targets and cleaves DNA are relatively well-understood, as numerous crystallization and bio-structural experiments have recently been published[94,95]. Cas9 forms a complex with a single guide RNA (hereafter referred to as gRNA). The complex scans the cell's genome for a short 2-6 nucleotide sequence called the protospacer adjacent motif (PAM). Cas9 proteins from different bacterial species recognize different PAMs. If the targeting sequence in the guide RNA matches the sequence upstream of a PAM, the Cas9 complex unwinds the genome DNA using complementarity binding from the guide RNA. An R-loops then forms with the gRNA and target DNA, and the HNH and RuvC nuclease domains within Cas9 cleave the complementary and noncomplementary DNA strands, respectively.

When Cas9 cleaves DNA in eukaryotic organisms, the resulting double stranded breaks are repaired by either error prone non-homology end joining (NHEJ) or homology directed repair (HDR) mechanisms. For gene therapy considerations, both repair pathways can be utilized depending on the desired outcome. The error-prone NHEJ occurs more frequently, and almost exclusively in non-dividing cells. NHEJ causes random insertion deletion mutations (indels) at the CRISPR targeting locus and can be used to disrupt coding sequences of desired genes [1,91,93]. Disruption of the coding sequence will generate premature

stop codons and activate nonsense mediated decay pathways which will destroy nascent pre-mRNA and silence gene expression (Fig. 3). HDR, occurs with a lower frequency in dividing cells, and can be used to insert a donor DNA template at the target site for precise editing[92]. The two outcomes give CRISPR a flexibility in designing gene therapies.

CRISPR is not the first nor the only gene-based technological platform for gene-therapy considerations. Other gene editing technologies such as meganucleobases, zinc finger nucleases, TALENs, have been previously designed and conceptualized for gene therapy. Utilization of these technologies, however, is difficult; since targeting different areas of the genome requires reconfiguration of the protein nuclease. Therefore, designing these technologies to target different sites in the genome is cumbersome, and strategies to build gene therapies based on these technologies is generally not scalable. Gene therapies using CRISPR, on the other hand are much simpler to design and scale since they use one single invariable protein and one programmable RNA strand.

Other gene therapy technological platforms which work by targeting RNA also exist and are used for gene therapies. These include RNA interference (RNAi)-based strategies and antisense oligonucleotide (ASO)-based strategies. RNAi strategies utilize endogenous nuclease AGO2 to suppress and cleave RNA, and ASOs utilize endogenous RNAse H to cleave RNA. When compared to other gene silencing technologies, such as RNAi and ASOs, Cas9 targets the

genome, not the transcriptome, allowing for permanent alteration. From a therapeutic perspective, one single delivery can permanently silence a gene via transient expression of the editing machinery. This in contrast with other therapies what need repeated injections to remain beneficial

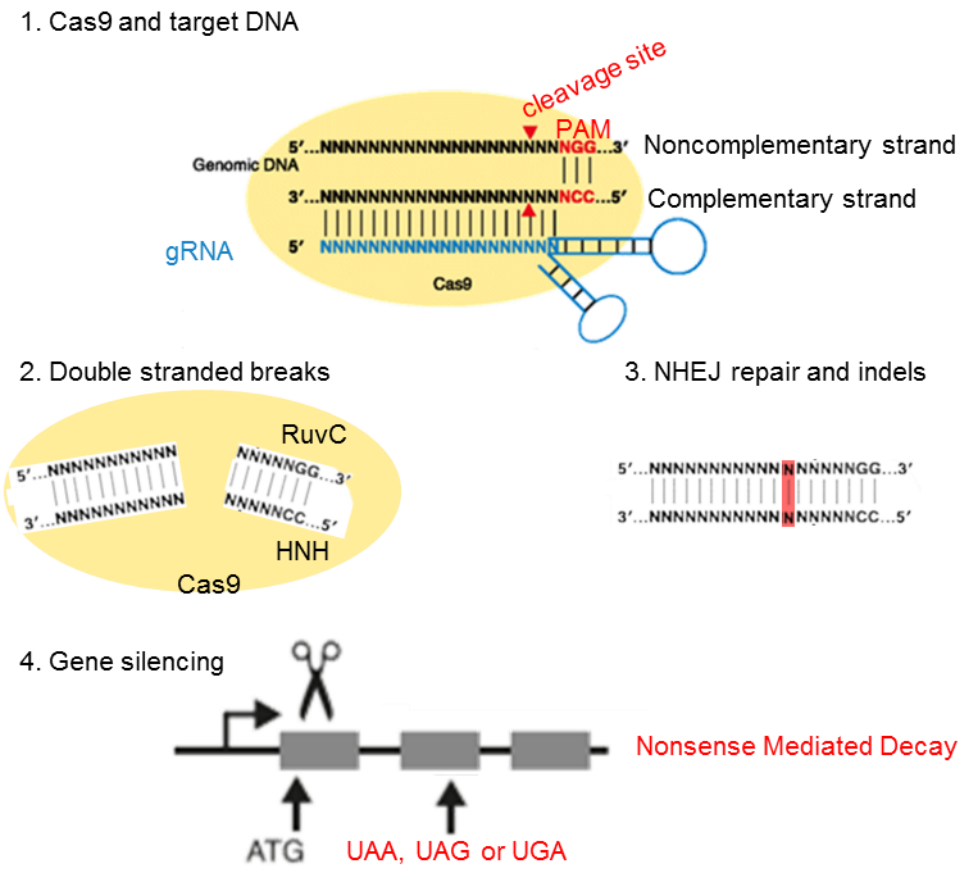

Figure 3. DNA repair via non-homologous end joining DNA repair generates insertions and mutations.

1. Cas9, guide RNA, and target DNA in complex. If the complementary sequence is immediately upstream of a PAM sequence, the gRNA forms and R-loop with the complementary target DNA strand enabling double stranded cleavage a few nucleotides upstream of the PAM. **2.** The RuvC domain of Cas9 cleaves the noncomplementary strand and the HNH domain of Cas9 cleaves the complementary strand **3.** NHEJ repairs cleaved DNA, often generating indels, in this case an insertion is shown in red. **4.** If indels are within coding

sequence, frameshifting occurs, generating premature stop codons downstream from cleavage site. premature stop codons will activate nonsense mediated decay and silence gene expression.

The CRISPR genome editing system has been demonstrated to work in the brains and spinal cords of mammals[96,97], and thus could be used to treat numerous genetic disorders of the central nervous system, including ALS.

One disadvantage of Cas9 as a gene therapy platform is the unknown effects associated with permanent gene editing. Much more work needs to be done to assess potential off-target effects of Cas9. Additionally, after injection of Cas9 there would be no way to stop or reverse silencing, in the event of an adverse reaction.

Recently, *Staphylococcus aureus* Cas9 (SaCas9) was used to silence *SOD1* in mice[97]. The small size of SaCas9 is advantageous for *in vivo* delivery, yet it recognizes a long “NNGRRT” PAM that limits the number of available PAMs in the genomic region of interest. By contrast, *Streptococcus pyogenes* Cas9 (SpCas9) recognizes a short “NGG” PAM that enables a larger selection of target sites in the gene of interest. Developing an *in vivo* delivery platform for SpCas9 will expand the genome editing toolkit for studying ALS.

1.5 Adeno-associated virus as a delivery vector

AAVs are small, single-stranded DNA viruses within the phylogenetic viral family *Parvoviridae*. AAVs are well-suited as vectors for gene therapy because of their broad tropism, low immunogenicity, and ability to infect non-dividing cells[98]. AAVs are well-established for use in therapeutic interventions, are currently being investigated in numerous clinical trials, and have been approved for use for a therapy to treat the neurological disorder spinal muscular atrophy[99,100]. The demonstrated efficacy and safety profile of AAVs make them ideal for use in delivering a CRISPR-based strategy to silence *SOD1* in the CNS.

Structurally, AAVs lack a membrane envelope but have a protein capsid. These capsids comprise 60 protein subunits arranged in icosahedral symmetry. Serotypes of AAVs are largely defined by differences in the structure of their capsids. Different capsids have different tissue and cell tropism. There are over a hundred known natural AAV capsids that infect humans and other primates[101].

The AAV genome consists of two genes, (each with their own promoter), *rep* and *cap. Rep* protein isoforms are involved in replication and *cap* protein isoforms are involved in capsid formation and capsid development. The genome is flanked by inverted terminal repeats, which play a role in many functions including encapsidation, DNA synthesis, and concatenation/circularization into episomal DNA following infection[102,103]. The size of the AAV genome is approximately 4.7kb.

The mechanisms by which AAVs infect cells are not fully understood. AAVs adhere to host cell plasma membranes by interacting with membrane glycans. Different AAV capsids preferentially bind to different glycans and different receptors. For most capsids, endocytosis is mediated by the host cell AAV receptor (AAVR), a transmembrane protein that interacts with AAV particles via an Ig-like polycystic kidney disease domain[104,105]. Endosomes containing AAVs are then trafficked to the trans-Golgi network via a microtubule-mediated mechanism after which the AAV particles escape the endosome by using the phospholipase capsid protein VP1[106]. From the cytoplasm, it is thought that the AAV particles are trafficked to the nucleus by importin-β[107] (see Fig. 4).

AAV vectors, have had the viral *rep* and *cap* genes replaced with therapeutic factors. As such, AAV vectors have a no ability to replicate and integrate into the host genome, and thus confer an increased degree of suitability for gene therapy. Further efforts have been utilized to increase engineering strategies that have been developed to produce better AAVs for gene therapies. Such examples include hybridizing and/or designing new capsid proteins and changing ITRs sequences to improve transcription.

Numerous experiments have been designed using AAVs to deliver RNA interference cargo (i.e., shRNA or miRNA) into mammals. More recently, efforts to delivery Cas9 machinery via AAV have ramped up.

1.6 Challenges using rAAVs to delivery CRISPR therapeutics

Challenges of using AAVs to deliver gene therapy include the small genome size, distribution and cell-specificity of the AAVs, ability to sufficiently transcribe cargo, and immunogenicity of AAVs in human populations.

AAV genome size: The AAV's small genome size constrains the amount of cargo it can deliver. When considering designing a RNA interference-based strategy, the small cargo size is not problematic. When delivering a CRISPR-based strategy, however, the small genome size becomes a challenge. Co-expressing the canonical *Streptococcus pyogenes* Cas9 (with a genome size of 4.3kb) along with sgRNA and all requisite regulatory elements in the same AAV vector exceeds the genome size of the AAV. To overcome this, smaller Cas9 proteins have been employed [97,108], or delivery of Cas9 and sgRNA can be split onto multiple AAVs.

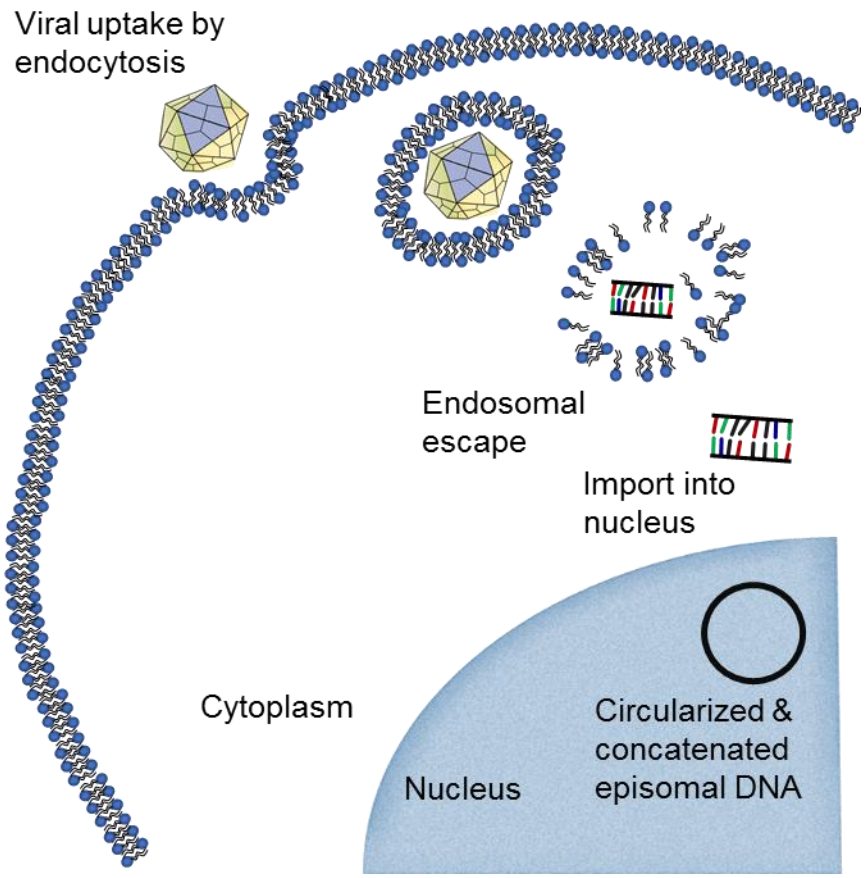

Figure 4. AAV transduction and nuclear localization.
AAVs bind to cell surface through glycan-capsid interactions. Endocytosis is mediated by AAVR1. AAVs escape endosome and are imported to nucleus. AAV DNA persists as circularized and concatenated episomal DNA.

Distribution and cell specificity: To be an efficient in gene therapy, AAVs must reach to and infect the desired tissue and cell type. Much research has been employed to develop different AAV capsids and different routes of injection, to confer tissue and specificity. Designing strategies to target tissue within the CNS, the blood-brain barrier confers is a major consideration. To this effect, researchers have employed AAV capsids that can cross the blood-brain

barrier (e.g., AAV9 or rhAAV.10) [109],[110] , or have administered AAVs directly into the CNS (e.g., via intrathecal, stereotaxic, or intracerebroventricular injections) [96].

Transcriptional Strength: All vehicles used to delivery nucleotide-based therapies (i.e., AAVs, lentivirus, lipid nanoparticles, etc.) faces similar challenges in maximizing/optimizing transcriptional efficiency of the cargo. Much research has focused on the characterization and optimization of regulatory elements, including promoters, polyA signals, and post-regulatory elements. One challenge specific to AAVs is slow transcriptional kinetics. Since AAVs comprise a single-stranded DNA genome and lack a polymerase gene, they require host cell machinery for priming and transcription, which results in slow transcription kinetics and comparatively weak expression. One method to increase efficiency includes the use of self-complementary AAVs, which bypass the rate limiting second-strand replication necessary for AAV transcription. This forgoes the need for host-machinery mediated second-strand replication and thus, achieves faster onset of transcription [111,112].

Immunoreactivity in human populations. Previous exposure to natural AAV infections can generate an immune response that can hamper AAV-mediated gene therapy. Both humoral and cell-mediated responses to AAVs have been detected. Humoral responses to AAVs include circulating neutralizing antibodies that limit cell transduction[113]. Cell-mediated responses to AAVs include a $CD8^+$ T Cell response that can cause both a loss of transduced cells and adverse inflammation[114].

Neutralizing anti-AAV antibodies have been found in all human populations [115]. Most individuals carry anti-AAV neutralizing antibodies that recognize some AAV capsids[100]. Antibodies against AAV1 and AAV2 are the most common and are found in nearly 70% of the human population, followed by antibodies against AAV6 and AAV9 which are found in nearly 45% of the human population[10].

Efforts to overcome the challenge of AAV immunoreactivity include screening for anti-AAV titers and immunosuppressing patients before AAV treatment. Delivery of AAVs to immune-privileged areas such as the CNS, however, may not be inhibited by an immune response.

In summary, despite many challenges, AAVs are among the most practical delivery vectors for gene therapy, They have previously been used to deliver Cas9 and guide RNA into the CNS in animal models and have a record of safety in clinical trials.

1.7 Rationale

ALS is a uniformly fatal neurodegenerative disease for which there is no cure. Mutations in the gene *SOD1* cause a subset of ALS cases, and are well characterized by animal models. Designing AAV-based, systemic and localized strategies to silence *SOD1* will help in the development of a therapy for *SOD1* ALS.

Chapter II Methods

2.1 Plasmid Construction

We designed sgRNAs targeting the human *SOD1* using the CRISPR DESIGN tool from MIT (crispr.mit.edu), which ranks all possible guides given a target genomic input based on predicted faithfulness of sgRNA (see Table 2 for sequences). All oligonucleotides encoding the sgRNA sequences were synthesized by Genewiz. For *in vitro* screening, we cloned our guide vectors into the lentiCRISPRv2 Cas9-FLAG-2A-Puro (Addgene 52961). For cloning, we phosphorylated our oligos using PNK (NEB), digested the plasmid backbone with BsmBI, and ligated with T4 DNA ligase (NEB). For plasmids packaged into AAV vectors, we cloned our gRNA oligos into the pAAV-U6sgRNA_hSyn-GFP-KASH-bGH plasmid (Addgene 60958, a gift from the Feng Zhang lab) via SapI restriction digestion. pAAV-pU1A-spCas9-RBGpA Cas9 plasmid was a gift from the Guangping Gao lab.

Oligonucleotide Type	ID	Sequence (5' to 3') or Plasmid Name
sgSOD1 sequence-Lead candidate for intravenous injection	1657 sghSOD1.E2c	AATGGACCAGTGAAGGTGTG
sgSOD1 sequence-LC ICV injection	sg.10	CCTCTATCCAGAAAACACGG
sgSOD1 sequence	sg.C	ccgtgaaaagaaggttgttt
sgSOD1 sequence	sg.D	CGGCGTGGCCTAGCGAGTTA
sgSOD1 sequence	sg.E	TCTGGCCTATAAAGTAGTCG
sgSOD1 sequence	sg.F	GTGGGCCAAAGGATGAAGAG
sgSOD1 sequence	sg.G	tgagtaacaaatgagacgctg
sgSOD1 sequence	sg.J	TTGCAGTCCTCGGAACCAGG
sgSOD1 sequence	sg.E2A	AGCATTAAAGGACTGACTGA
sgSOD1 sequence	1657 sghSOD1.E2c	AATGGACCAGTGAAGGTGTG
sgSOD1 sequence	SG.9	AATCCTCTATCCAGAAAACA
sgControl sequence*	sgLacZ(Addgene 60228)	TGCGAATACGCCCACGCGAT
SOD1 genotyping primer	mSOD fwd	GCATACCCAATCACTCCACAG
SOD1 genotyping primer	mSOD rev	GTCCATGAGAAACAAGATGAC
SOD1 genotyping primer	hSOD fwd	CATCAGCCCTAATCCATCTGA
SOD1 genotyping primer	hSOD rev	TCTTAGAAACCGCGACTAACAATC
Sequencing library primer	1811 SOD1exon2.F	CCATCTCCCTTTTGAGGACA
Sequencing library primer	1812 SOD1exon2.R	CGACAGAGCAAGACCCTTTC
backbone AAV-sgRNA	Addgene 60228	AAV:ITR-U6-sgRNA(LacZ)-pCBh-Cre-WPRE-hGHpA-ITR
backbone AAV-sgRNA	Addgene 60958	pAAV-U6sgRNA_hSyn-GFP-KASH-bGH
backbone-AAV Cas9	AAV.Cas9	pAAV-pU1A-spCas9-RBGpA Cas9
backbone-Lenti sgRNA/Cas9	Addgene 52961	lentiCRISPR v2

'* initially published in *Platt, R. J. et al. CRISPR-Cas9 Knockin Mice for Genome Editing and Cancer Modeling. Cell 159, 440–455 (2014).*

Table 2. Oligonucleotides used for the design, development and optimization of AAV-mediated targeting of SOD1

2.2 Lentivirus packaging

For generation of sgSOD1 lentivirus, we used lentiCRISPRv2-Cas9-Flag-2A-Puro plasmids (see Table 2 for Addgene requisition numbers). HEK293fs were seeded in 6-well plates to a density of 70%. Cells were then transfected with lentiCRISPRv2-Cas9-Flag-2A-Puro-sgSOD1 along with Δ8.2 and VSVG helper plasmids. Supernatant containing virus was collected at 36, 48 and 60 hours. Viruses were purified by passing supernatant through a 0.45um Whatman filter (GE). Viruses were either frozen at -80ºC or used immediately by dropping them onto human carcinoma HCT116 cells that were seeded at 70% confluence. Polybrene was added to the infected cells immediately after infection.

2.3 Cell culture

We maintained all cell lines at 37C and 5% CO_2. For initial screening, human carcinoma HCT116 cells RNA were maintained in DMEM supplemented with 10% FBS. HCT116-sgSOD1-Cas9 cell lines were generated by infection with lentiCRISPRv2-Cas9-Flag-2A-Puro.sgRNA lentivirus. For *in vitro* testing of the AAV9 vectors, human embryonic kidney HEK293T cells were maintained in DMEM supplemented with 10% FBS.

2.4 Surveyor and T7 assays

We transfected both HEK293T and SH-SY5Y cells as follows: We seeded cells to a density of 70% and transfected them using the TransIT LT1 transfection

kit (Mirus Bio). After 72 hours we isolated DNA using QuickExtract™ DNA Extraction Solution (Epicentre). We amplified the *SOD1* locus using Herculase II polymerase and primers we previously designed (Table s1). Both the Surveyor mutation detection kit (IDT) and the T7 endonuclease kit (NEB) were used to check for indels. We detected cleavage products by gel electrophoresis using a Tris-Borate 10-12% gel

2.5 Tracking of Indels by Decomposition (TIDE) analysis

DNA was isolated and amplification of the *SOD1* locus was done as described above. Amplified DNA was Sequenced using Genewiz using the forward and reverse primers (Table 2). Trace files were used to quantify Indel percentage using TIDE (https://tide.nki.nl/).

2.6 Mice

All mouse work was approved by IACUC (Docket# A-1984-14-9). All mice were housed in the UMASS Medical School Albert Sherman Center vivarium. All mice had constant access to food and water. For facial vein injections, we crossed *SOD1*^{G93A} mice (B6SJL-Tg(SOD1*G93A)1Gur/J, Jax 002726) with either B6;129-Gt(ROSA)26Sortm1(CAG-cas9*,-EGFP)Fezh/J Jax 024857) or STOCK Gt(ROSA)26Sortm1.1(CAG-cas9*,-EGFP)Fezh/J Jax 024858) Cas9 knockin mice to create double transgenic mice. For ICV injections we used

SOD1^{G93A} mice (B6SJL-Tg(SOD1*G93A)1Gur/J, Jax 002726). For both studies, animals were injected and observed by blinded personnel.

All mice with human mutant *SOD1* were monitored daily for signs of neurodegeneration. After signs of degeneration, mice were provided gel water and moistened food. For survival studies, endpoint was defined as the time point when a mouse when they cannot right themselves (go from a lateral position to a ventral position) from one side in less than 10 seconds. Mice were sacked at endpoint according specifications in the IACUC protocol.

2.7 Facial vein injections

The protocol was adapted from published literature[116]. Mice, aged p1-p3, received up to 2x10e12 genome copies (gc) AAV in PBS solution or PBS in a maximum volume of 50ul PBS through the facial vein. Prior to injection, mouse pups were anesthetized by placing them on a rubber glove atop wet ice for 30-60 seconds until no longer moving. Anesthetized mice were then placed under the microscope and a 30G needle was used to deliver the vector. The needle was inserted bevel-side up and 50 or 100ul volumes was used to deliver the vector. After injection, mice were rewarmed by hand for 2-3 minutes. To prevent rejection by the mother, pups were covered with bedding material, and the mother's nose was dabbed with a Kim wipe soaked in ethanol. When necessary, a portable hand warmer or recirculating water heating pad was used to rewarm

the neonates. Following injection, neonates were monitored closely during the first 24 hours for possible rejection by the mother.

2.8 ICV injections

All experiments were performed at the University of Massachusetts Medical School and were approved by the Institutional Review Board. Male B6SJL-Tg(SOD1-G93A)1Gur/J (Jackson Laboratory, Bar Harbor, ME; stock# 002726) and female non-transgenic (NTG) littermates were used to breed mice. AAV9.Cas9 and AAV9.guide vectors were mixed together and then injected into the cerebral lateral ventricles of postnatal day 1 (P1) mice as described by Stoica *et al*[72]. Undiluted stock concentrations were 8e9/ul for the AAV9.cas9 vector and 9e9/ul for the AAV9.guide vector. Untreated *SOD1*^{G93A} mice, AAV9.Cas9 treated *SOD1* mice, and AAV9.nontargeting guide+AAV9 treated mice were used as controls. Mice were observed weekly for signs of paresis/paralysis and sacked at disease endpoint, defined by the inability for a mouse to right themselves after being placed on their back within 10 seconds. Mice were euthanized and immediately frozen or fixed in 10% formalin or 2.4% glutaraldehyde. Three mice from five mice from the Cas9+sgSOD1 group and three mice from the Cas9+sgControl group and the Cas9+sgSOD1 group were sacrificed at disease midpoint, 110 days, for histological and biochemical studies. At day p85 and

p110, mice from the sgSOD1 group and untreated *SOD1* group were used for net axonal transport measurements.

2.9 Grip strength performance:

We monitored the evolution of clinical weakness using the grip-strength meter (Mark-10, USA). This device measures the strength of both the hind limbs and fore limbs of the mice. Grip strength testing was performed in a unidirectional air flow hood. Mice were positioned such that they could grip the meter, and then were gently pulled back away from the meter, generating a force measurement. Grip strength from the forelimbs and from all limbs were assessed. There is no risk of injury for the mice during these tests. Mice were acclimated for 2 weeks before recording results. Testing occurred once a week.

2.10 Rotarod motor performance:

We monitored the evolution of clinical weakness of mice by using a rotarod device (Omnitech Electronics). Rotarod testing of all experimental and control animals began at 90 days post-birth. Rotarod testing was performed in a unidirectional air flow hood in AS-1061 Procedure Room (see Section A7). Rotarod testing sessions were performed twice per week, with 2-3 days between tests. The Rotarod was set to a speed of 15 revolutions per minute, and animals were run on the rotating rod for a maximum of 300 seconds 3 trials were performed per session with minimum of 10minutes rest between each trial.

2.11 Weight and paresis

Mouse were weighed weekly and the degree of paresis was assessed by the following scoring system: 1; upon lifting mouse by tail, mouse fully abducts hind limbs. 2; upon lifting mouse by tail, mouse abducts hind limbs, paws face outwards. 3; Upon lifting mouse by tail 'clasping' observed, lack of hind limb abduction, paws no longer face outward and face behind. 4; Severe Clasping and waddling and dragging rear quarters behaviors. 5; paralysis in one or more limb.

2.12 Deep sequencing

Deep sequencing was performed using the ILLUMINA MiSeq kit. Genomic DNA from end stage Cas9+guide treated and end stage NT+Cas9 treated mice were extracted using the High Pure PCR template Preparation Kit (Roche). Each site was amplified by PCR using Phusion Flash polymerase. Custom barcodes were incorporated into via a second PCR. PCR products were purified using the Qiagen PCR purification Kit. Barcoded amplicons were pooled together and sequenced using the MiSeq DNA sequencer (Illumina). Reads were sorted by barcode, filtered for >99% confidence (phred33 ≥ 20) per read. Indel quantification was done using CRISPResso[117]

2.13 Quantification of ventral root axons

Mid-disease mice (p110) were fixed by perfusion with 4% PFA in PBS and the L5 ventral nerve roots dissected. The ventral root samples were first fixed overnight in 2.5% glutaraldehyde in 0.1M cacodylate buffer, and then washed and post-fixed in 1% osmium tetroxide for 1 hour. Samples were then dehydrated through a graded ethanol series into propylene oxide, followed by overnight fixation in 1:1 solution of propylene oxide and SPI-Pon 812 rein mixture. Following a three-hour incubation, samples were polymerized at 68C for 4 days. Nerves were trimmed, reoriented and cut into 0.6um sections. These sections were mounted on glass plates, stained with toluidine blue, washed and mounted with a coverslip. Sections were then imaged, with axon number diameter and area quantified using ImageJ (National Institutes of Health, Bethesda, MD).

2.14 Neuromuscular junction staining

We perfused and fixed mice using 4% PFA as described previously. We cut 35μm thick sections of gastrocnemius. For staining, tissues were thawed, washed with PBS, permeabilized with PBS-0.4% TritonX and then blocked with 10% donkey serum in PBS-TritonX. Tissues were then incubated overnight with rabbit anti-synaptophysin (Invitrogen 080130) and rabbit anti-BIII tubulin (Covance, PRB-435P-100). Tissues were washed with PBS and incubated with Donkey anti-Rabbit and α-bungarotoxin diluted in PBS. Images were taken on Nikon microscope and visualized using ImageJ and Nikon Elements Viewer. A

blinded observer recorded and scored by eye each NMJ as either intact, partially denervated, or fully denervated. Three treated groups were scored, untreated, sgSOD1, and sgControl, n=3 mice for each group.

2.15 *In vivo* quantitation of net axonal transport.

Preparation of recombinant tetanus toxin fragment C (TTC) was prepared as follows: TTC was overexpressed and purified in Escherichia coli strain BL21 (DE3)[118], and radiolabeled by incubating 3 ug of TTC per mCi of ^{125}Iodine-radionuclide (^{125}I) (Perkin Elmer) for 10 minutes. Radiolabeling of TTC was then quenched with tyrosine.

In vivo imaging of net axonal transport was performed as follows: One week prior to imaging, mice were given water supplanted with potassium iodine to block baseline interactions with free 125I. For the imaging, mice were under isoflurane anesthesia during the entire procedure. ~100 ug of TTC was injected into the gastrocnemius at a rate of 10 ul per minute. Following the injection, animals were imaged on a NanoSPECT/CTTM small animal imaging camera (Bioscan Inc.) at twenty-four-hour intervals. The collected CT and SPECT images were reconstructed, and radioactivity at the region of interest was analyzed using VivoQuant 1.23 software (InvivoCRO). All imaging experiments and data analyses were performed blind.

2.16 Laser capture microdissection

Frozen, unfixed spinal cord tissue embedded in OCT was cut using a cryostat into 10µm thick sections. 8 sections were fitted onto one slide. Slides were stored at -80 until use.

All laser capture microdissection was performed using the Arcturus XT Laser Capture microdissection system. (Arcturus). Slides were thawed in 75% EtOH for 30 seconds, washed in ddH_20 for 30 seconds and then stained with Cresyl Violet. Slides were then dehydrated in graded ethanol solutions (75% EtOH, 95% EtOH, 100% EtOH, 100% EtOH, 30 seconds per solution) and cleared in Xylene for 5 minutes. Slides were then dried using handheld fan and mounted onto the microscope. For each sample, 300 motor neurons, identified by morphology and location within the ventral horn of the spinal cord, were dissected using the Infrared laser. The collection cap containing the micro-dissected motor neurons was placed upright on ice and 5µl RIPA buffer containing a protein inhibitor cocktail (Roche) was added. Considerate care was taken to ensure that all portions of the collection tube's surface area was immersed in RIPA. The caps were then placed in collection tubes, vortexed for 30 seconds, spun down and stored at -80 until further use.

Lysate was analyzed using the ProteinSimple Wes capillary western blot machine and normalized to total protein levels. Anti-goat SOD1 antibody was used to detect SOD1 (AF3418, R&D Systems) and total protein was assessed

using ProteinSimple Total Protein kit (ProteinSimple). for each sample two 3µl volumes were loaded into two lanes, with one lane detecting total protein and the other lane detecting SOD1. Results were visualized and analyzed using Compass SW software (version 4.4.0 ProteinSimple). To both quantity total protein and ensure that detection of total protein fell within the machine's limit of detection, a standard curve consisting of serially diluted whole brain RIPA extract was run alongside laser captured samples.

2.17 ELISA

Tissue samples were lysed in RIPA buffer with a protein inhibitor cocktail (Roche) and protein lysate isolated and stored at -80C. Lysates were then thawed on ice, and their concentrations were determined by BCA assays. Lysates were then diluted to 0.2ng/ul and assayed using a commercially-available sandwich ELISA for human SOD1 (Invitrogen).

2.18 digital droplet PCR (ddPCR) of LCM motor neurons

RNA from Laser-captured motor neurons in lumbar and thoracic spinal cord sections were isolated using Arcturus Pico Pure RNA isolation kit. RNA was converted to cDNA using Multiscribe^{tm} RNA transcriptase (ABI) kit. cDNA from 150 motor neurons were analyzed per section. Tissue from the dorsal horn was dissected from each spinal cord section and served as an internal control. Sample cDNA were processed into droplets and run on the Bio-Rad QX100

ddPCR system according to the manufacturers' protocol. Results were analyzed using Quantasoft^{tm} Analysis Pro software (Bio-Rad).

2.19 Statistical analysis

For ELISA, Grip strength, Neuromuscular junction analyses, and ddPCR t-tests were used to compare sgSOD1 mice and control cohort. For survival analysis of CRISPR-Cas9 treated mice, differences Kaplan Meir curves were determined by log rank test. For comparison of correlation between Age of onset and duration of disease, significance was determined by Fischer's z to r test.

For ventral root axon diameter analysis, statistical significance was determined by one-way ANOVA using the Holm-Sidak method for correcting for multiple correction. Motor neurons that we ascribed as having a diameter of 4um and greater, were analyzed and a $P< 0.05$ was regarded as significant.

For net axonal transport Statistical significance was determined by two-way ANOVA after Bonferroni's correction, with $P < 0.05$ being regarded as significant. The P values for each experiment were determined and stated in the figure legends. To determine the associations between disease stage/age with peak amplitude or between disease stage/age with time-to-peak values, linear regression was used to generate trendlines with R^2 values stated in the figure legends.

For gel capillary western blot, statistical significance was determined by unpaired student's t-tests.

Chapter III Systemic delivery of sgRNA targeting *SOD1* prolongs survival in transgenic mice expressing Cas9 and $SOD1^{G93A}$

3.1 Preface

I conceptualized the project under mentorship of Dr Robert Brown and Dr Wen Xue. I designed sgRNAs using MIT.CRISPR.edu and by manual review. I synthesized and cloned all sgRNAs. I performed all cell culture, qPCR, western Blot, TIDE and Surveyor Assays. For all preceding experiments I was assisted by Haiwei Mou. For cell culture assays, I was assisted by Suetyan Kwan. Packaging of AAV plasmids into AAV9 virus was done by the Viral Core at Children's Hospital Boston. I performed additional QC on virus. I generated *SOD1* x Cas9 mice. Jia Lee performed facial vein injections. I performed genotyping, weight, grip strength, neuro-score, and rotarod assays. For all mouse work, I was assisted by Alexandra Weiss and Jake Metterville. I performed all animal harvests. I performed all tissue sectioning and was assisted by Alexandra Weiss and Jake Metterville. I performed all microscopy and was assisted by Haiwei Mou. For Western Blots, I was assisted by Tingting Jiang and Haiwei Mou.

3.2 Abstract

Genetic silencing of the *SOD1* is a promising strategy for therapeutic intervention of ALS. Mutations in *SOD1* are the most characterized genetic cause of ALS and account for ~20% of all familial cases. CRISPR-Cas9 technology, based on the programmable nuclease Cas9, can specifically and robustly silence genes by generating frameshift mutations within the coding sequence of a desired gene. Before CRISPR technology can progress to the clinic, strategies to deliver CRISPR components to the Central Nervous System need to be investigated. In this study, we assess the ability of *Streptococcus pyogenes* Cas9 to silence *SOD1* in the brain and spinal cord. We delivered via intravenous injection a guide RNA targeting *SOD1* into a transgenic mouse expressing human mutant *SOD1* and Cas9 using adeno-associated virus 9. (AAV9). We demonstrate on-target gene editing, increased survival, improvements in rotarod, grip strength and weight retention, and a trend for decreased *SOD1* mRNA expression in the brain and spinal cord. We also observe high levels outside the CNS, with exceedingly high levels of indels in the liver, which could be detrimental in a clinical application. We conclude that Cas9-mediated genome editing can mediate disease gene silencing in the CNS and warrants further development for use as a therapeutic intervention for *SOD1*-linked ALS patients.

3.3 Introduction

ALS is an adult-onset motor neuron disease that causes progressive degeneration in upper and lower motor neurons, leading to death usually within 3-5 years of onset. Approximately 90% of ALS cases are sporadic and 10% of cases of ALS are familial, in which one of numerous ALS associated mutations is inherited. Mutations in the free-radical scavenger gene *SOD1* are the second most prevalent genetic cause of Amyotrophic Lateral Sclerosis (ALS), accounting for ~20% of all inherited cases and 1-3% of all sporadic cases[13–16]. While the exact mechanism by which SOD1 causes neurodegeneration is unclear, numerous studies suggest that SOD1 protein misfolding and consequent aggregation contribute to cell death[16,119]. Interestingly, SOD1 misfolding is also observed in a subset ALS cases with no genetic *SOD1* mutation [15,20,32], suggesting wtSOD1 may contribute to pathology in a manner similar to mutant SOD1. These lines of evidence suggest that silencing *SOD1* could be potentially therapeutic in a subset of ALS cases, including cases that do not have a *SOD1* mutation.

Many animal studies have demonstrated that repression of *SOD1* through RNA interference (RNAi) ameliorates disease in animal models by delaying onset, prolonging progression, and increasing survival[14,23,72–74]. Yet, RNAi has limitations as a therapeutic, because delivery of RNAi molecules only transiently repress translation. For RNAi to be an effective therapeutic, either continuous expression of the RNAi molecule must occur in the brain and spinal cord, or

continual delivery of new RNAi vectors must be administered. Both present drawbacks in terms of developing a rationale therapeutic strategy to silence *SOD1*.

In contrast, the DNA-editing technology based on the type II CRISPR-associated Cas9 protein (Cas9) can complex with the bioengineered single guide RNA (sgRNA) and cleave DNA, leading to permanent silencing of gene transcription *in vitro* and in mammalian models[1,91,93]. Cas9 is guided to the target sequence by a complementary base pairing of the sgRNA and cleaves both strands of the DNA. A portion of the cleaved DNA is imperfectly repaired by non-homologous end joining (NHEJ) repair pathway, creating insertions or deletions (indels) at the target site. When targeted to the coding sequence of a gene, these indels disrupt the reading frame of the sequence, generating premature stop codons and driving degradation of subsequent mRNA by nonsense mediated decay (NMD). After DNA cleavage, Cas9 expression is no longer needed to silence genes and doesn't need to be continually expressed.

The permanence of Cas9 editing makes it advantageous over RNAi as a potential therapeutic, as one administration of sgRNA and Cas9 could potentially rectify genetic disorders. However, several drawbacks remain. Currently utilized Cas9 proteins have demonstrated 'off-target' cleaving, where sites of DNA that have near-complementary to the 5' end of the sgRNA are targeted. Additionally, the generation of indels at the targeted site cannot be precisely controlled and may cause missense mutations, which would not silence gene expression and

express a mutant isoform of the target gene. These considerations taken with the challenges associated with delivery to specific tissue make it clear that gene therapy approaches involving Cas9 need more investigation. *SOD1* is an excellent candidate as a target for a Cas9 translational study, as there is both a clinical need and a wealth of previous literature describing the outcomes of *SOD1* repression in mouse models.

3.4 Results

3.4.1 Design of sgRNAs and AAV packaging

We designed sgRNAs within the first four exons of the human *SOD1* locus using CRISPR.MIT.edu that finds and ranks sgRNAs algorithmically based on lowest probability of off target-sites (Fig. 5A). We selected an sgRNA sequence that did not overlap the most common mutant *SOD1* gene mutations found in patient populations (Fig. 5B). We then cloned the sgRNAs into the Cas9-containing plasmid px330 (Addgene 42230). We tested sgRNA indel efficiency by transfecting the human carcinoma cell line HCT116 and then performing Surveyor mutation detector assays (Fig. 5C).

To determine whether our sgRNA could work *in vivo,* we first generated a transgenic mouse model that expresses both human mutant *SOD1*^{G93A} and Cas9 (generated from Jax mice stock number 002726 and 024857) (Fig. 5D). We then cloned the sgRNA into an AAV plasmid (Addgene 60229), which controls sgRNA under a U6 promoter, and CRE under control of a BBH promoter and packaged

them into AAV9 viruses (Fig 5.E top) .We injected via intraperitoneal injection our AAV9 expressing sgSOD1 into a transgenic mouse model and sacked mice after 3 weeks (Fig. 5E bottom). We found formation of indels at the predicted *SOD1* locus in the liver and pancreas (Fig. 5E bottom right).

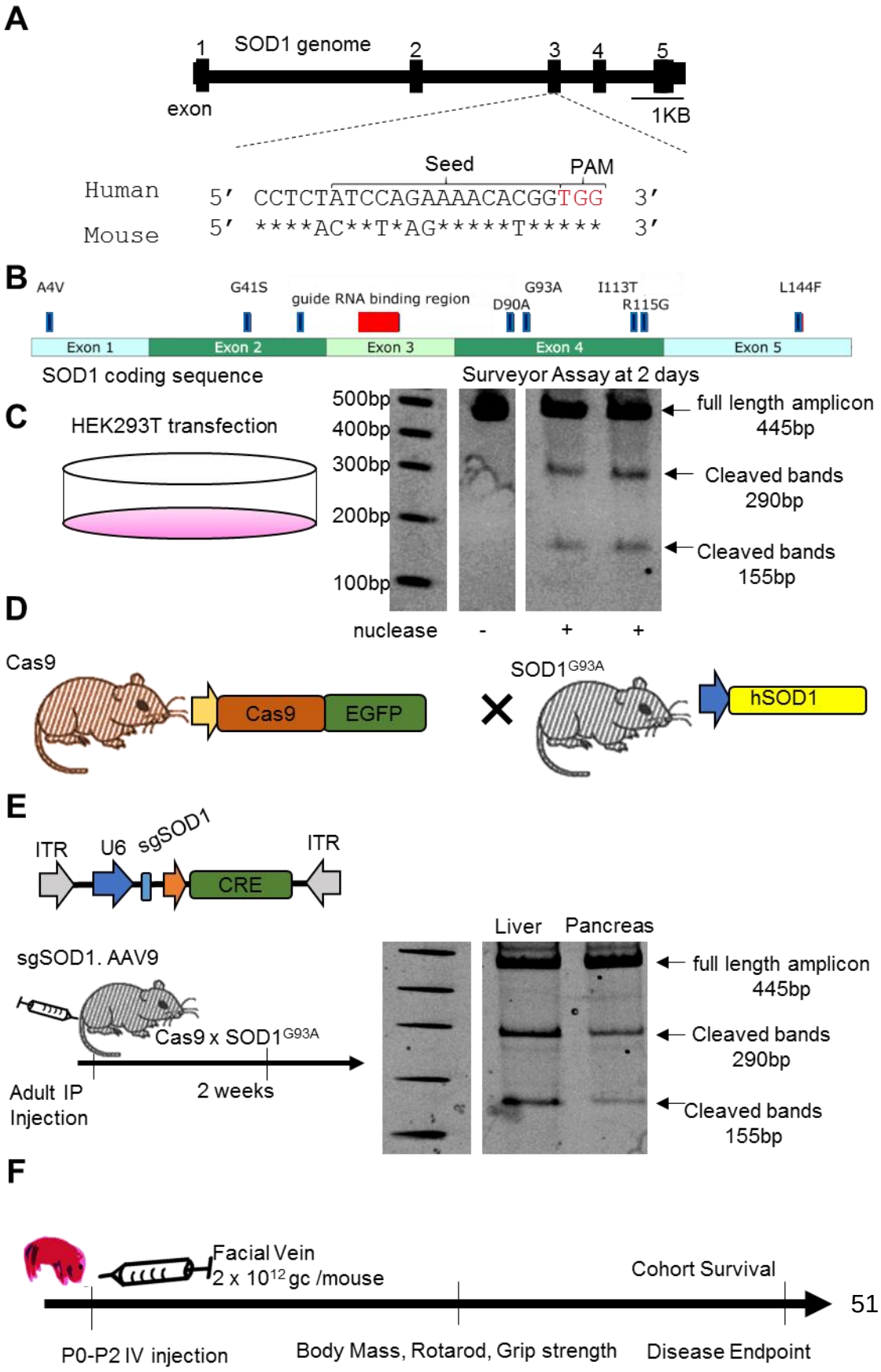
A
SOD1 genome
1
2
3
4
5
exon
1KB
Seed
PAM
Human 5′ CCTCTATCCAGAAAACACGGTGG 3′
Mouse 5′ ****AC**T*AG*****T***** 3′
B
A4V
G41S
guide RNA binding region
D90A
G93A
I113T
R115G
L144F
Exon 1
Exon 2
Exon 3
Exon 4
Exon 5
SOD1 coding sequence
C
HEK293T transfection
Surveyor Assay at 2 days
500bp
400bp
300bp
200bp
100bp
full length amplicon 445bp
Cleaved bands 290bp
Cleaved bands 155bp
nuclease - + +
D
Cas9
Cas9
EGFP
SOD1G93A
hSOD1
E
ITR
U6
sgSOD1
CRE
ITR
sgSOD1. AAV9
Cas9 x SOD1G93A
Adult IP Injection
2 weeks
Liver
Pancreas
full length amplicon 445bp
Cleaved bands 290bp
Cleaved bands 155bp
F
Facial Vein
2 x 10^12 gc /mouse
Cohort Survival
P0-P2 IV injection
Body Mass, Rotarod, Grip strength
Disease Endpoint

Figure 5. CRISPR-mediated editing of human *SOD1*

(a) sgSOD1 targets the third exon of human SOD1. **(b)** Schematic of common SOD1 mutations found in ALS patients and targeting region of sgRNA. **(c)** Surveyor Assay of stably infected HEK293T cells stably expressing Cas9 and sgRNA. Band at 445bp is the PCR product of the SOD1 locus. Cleavage bands indicate the presence indel mutations. **(d)** Generation of double transgenic human $SOD1^{G93A}$ x Cas9 mice. **(e)** Schematic of AAV plasmid used for in vivo studies. sgRNA is under control of a pol III U6 human promoter. **(f)** *In vivo* experiment design. 1-3-day old $SOD1^{G93A}$ x Cas9 transgenic mice received $2x10^{12}$ AAV vector delivered into the facial vein. Mice were monitored weekly and until endpoint.

3.4.2 Survival and motor function Improvements

To determine if our sgRNA could edit *SOD1* in the CNS and to assess survival and functional outcome, mice were injected intravenously with sgRNA through their facial vein within 2 days of birth with 2E12 gc vector (n=15) and monitored for survival (Fig. 5F). For controls, we used un-injected Cas9:*SOD1* mice, injected $SOD1^{G39A}$ mice (i.e. littermates, that lack the Cas9 transgene), and un-injected littermates that lack the Cas9 transgene (total n=10). Mice were also monitored daily with weekly weight, grip strength and rotarod assessments recorded. Compared to control groups, treated mice had increased median survival (Fig. 6A, 145.5 days vs 127, $p<0.0001$). Compared to controls, treated mice had improved weight retention starting at week 17 (Fig. 6B). Treated mice also had a delay in disease onset as measured by observation of hindlimb clasping (Fig 6C 129 days vs 113 days, $p=0.004$). Motor improvements were also

observed through both rotarod performance starting at week 17 (Fig. 6D, mean time to fall 130 sec vs 62 sec p=0.0013), and grip strength starting at week 16 (Fig. 6E, maximum force generated 1.04N vs 0.78N, p=0.033).

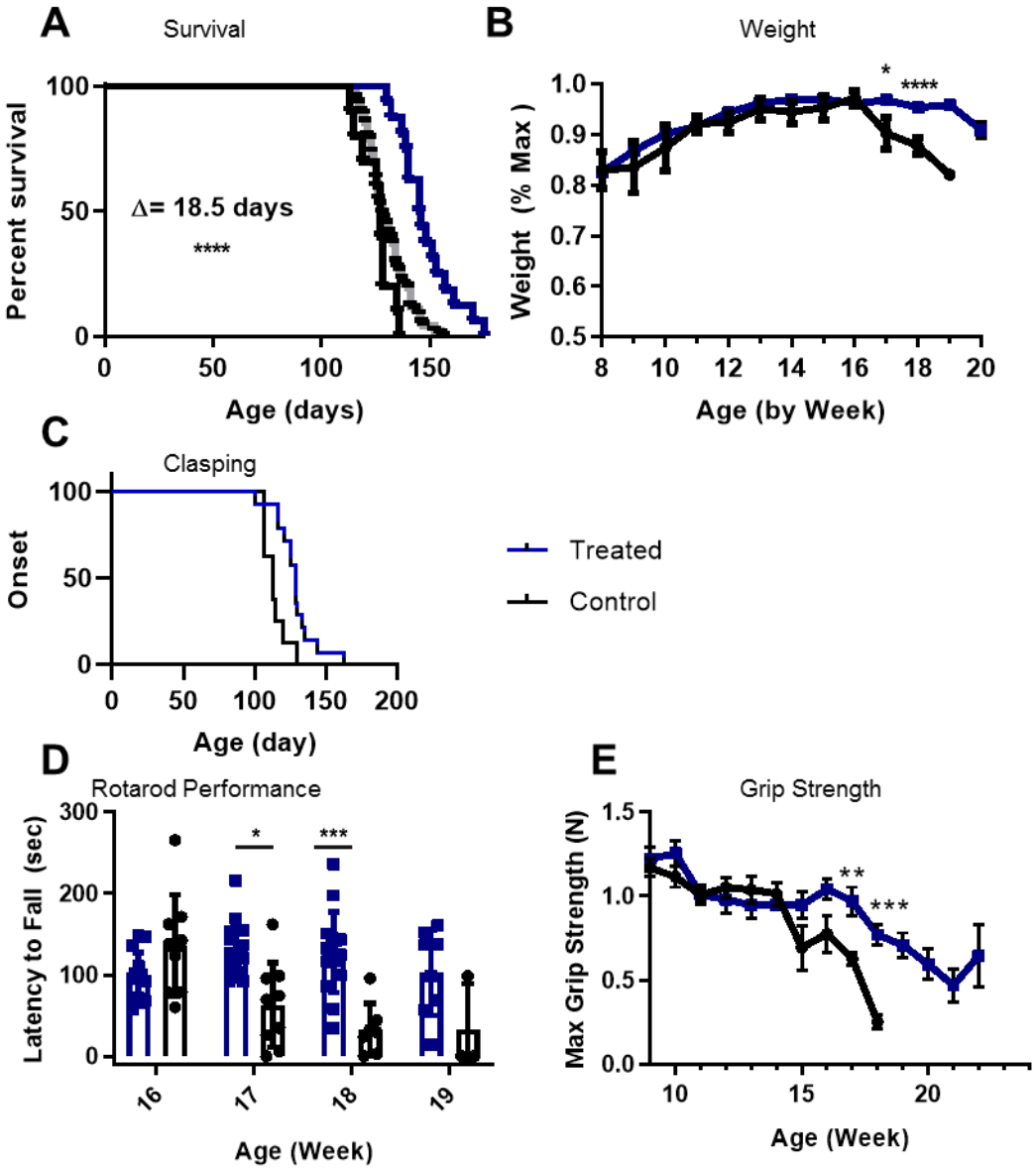

Figure 6. Targeting SOD1 increases survival in *SOD1^{G93A}*; Cas9 mice

SOD1^{G93A} x Cas9 mice were injected intravenously through their facial vein within 2 days of birth with 2E12 gc vector and were monitored daily. **(a)** Median survival for treated mice (n=16) was 145.5 compared to 127 to mice in the control group (n=10). p-values for Mantel-Cox Log Rank test was p<0.0001. **(b)** Average weights of treated mice compared to mice in the control group, with significant differences observed at weeks 16, 17 and 18, p-values=0.0223, 0.0001, and <0.0001, respectively. **(c)** Kaplan Meir graph of onset of clasping phenotype, an observable measure in which mice can no longer fully abduct hindlimbs after lifting them by their hindlimbs. Median age for onset of clasping phenotype for treated mice was 129 days compared to 113 days for control, p=0.004. **(d)** Rotarod testing of treated mice showed differences in latency to fall at weeks 17 and 18 compared to mice in the control group, p-values =0.0007, and 0.004 respectively. **(e)** Max Grip strength decline is slowed in treated mice compared to controls at week 16 and 17 p-values =0.0013 and 0.0001, respectively.

3.4.3 Detection of on-target indels by deep sequencing cortical and spinal cord tissue

To ensure that the survival and phenotype improvement was due to indel formation, we deep-sequenced the targeted locus within the *SOD1* locus. All indels observed in the brain and spinal cord that occurred with a frequency higher than 0.01% generated premature stop codons at one of four sites (Fig. 7A). Critically, all premature stop codons generated were upstream of the NMD boundary, a region +-50nts upstream of the last exon-exon junction after which premature stop codons no longer signal for nonsense mediated decay[120].

We detected indel frequencies of 3% in the spinal cord and 5% in the brain. In both the brain and the spinal cord, the most prevalent indel mutation was the insertion of adenosine 3 nucleotides upstream from the PAM (Fig. 7B and 7C). No indels that occurred with a frequency higher than 0.01% caused missense mutations, which would not be degraded by nonsense mediated decay.

To determine whether AAV9.sgRNA infected peripheral tissue, we sequenced DNA from the liver. We found high levels of editing in the livers, 76% (Fig 7B and C).

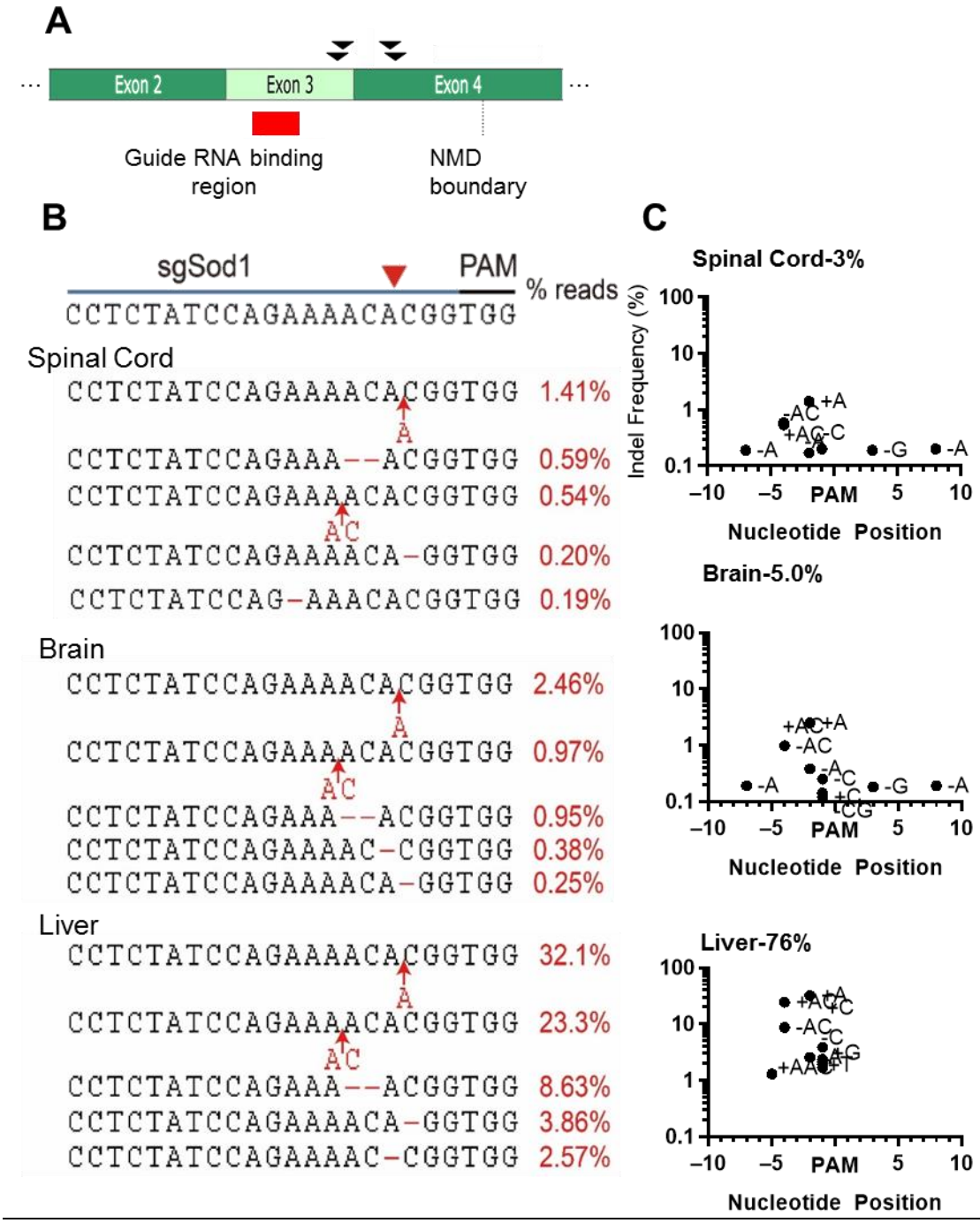

Figure 7. Indel formation in the brain and cpinal cord following facial vein injection of AAV9.sgSOD1

(a) Exon map of sgRNA binding location, premature stop codons generated by indel mutations, and NMD boundary within SOD1. **(b)** Sequencing reads and frequency of indels detected at sgRNA targeting locus. For the Brain, Spinal Cord and liver, the most frequent indel was the insertion of A three nucleotides upstream of the PAM. **(c)** Plot of frequency of individual indel versus location within SOD1 locus. All indels detected were upstream of PAM and generated premature stop codons and not missense mutations.

3.4.4 Decrease of *SOD1* transcripts in CNS

To determine whether AAV9.sgSOD1 reduces *SOD1* transcripts in the CNS spinal cord, we performed qPCR on endpoint cortical and lumbar spinal tissues. Compared to untreated mice, there was a ~31 percent reduction in *SOD1* transcripts in the brain (Fig. 8A, p=0.0173), and a 66 percent reduction in the lumbar spinal cord (Fig. 8B, p=0.0475). Additionally, in the lumbar spinal cord, we observed an increase in the standard deviation of qPCR results between sgSOD1 mice when compared to sgControl mice.

To assess whether our facial vein injection was permitting excessive viral transduction outside the CNS, we performed qPCR for *SOD1* on endpoint liver tissue. We found that treated mice had a 73 percent reduction in *SOD1* compared to mice in the control group (Fig. 8C, p=0.0078).

To determine whether AAV9.sgSOD1 reduces microgliosis, we measured transcript levels of the microglial-specific marker Ionized calcium binding adapter

molecule (Iba1) via qPCR on endpoint cortical tissue. We did not find a statistical difference in Iba1 levels between treated and untreated mice (Fig. 8B).

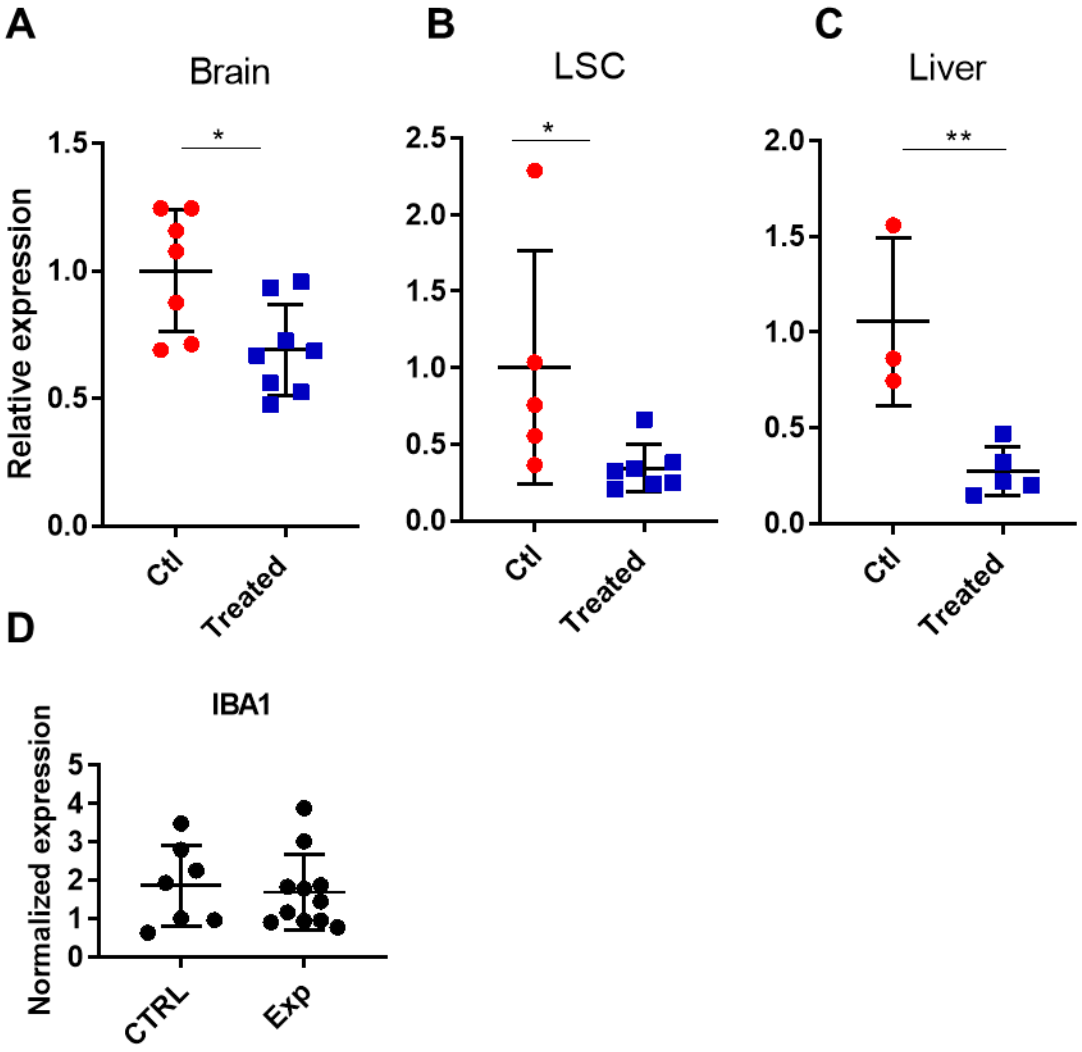

Figure 8. sgSOD1 reduces *SOD1* mRNA expression

(a -c) qPCR relative expression of SOD1 in control mice and in treated mice, in Brain (a), Lumbar Spinal Cord LSC **(b)** and in Liver **(c)**, p-values = 0.0173. 0.0475, 0.0078, respectively. **(d)** qPCR relative expression of microglial marker IBA1 in control and treated mice cortical tissues, p-value =0.719.

Chapter IV ICV CNS delivery via ICV injection of Cas9 and guide RNA targeting *SOD1* prolongs survival

4.1 Preface

I conceptualized the project under the mentorship of Drs. Robert Brown and Wen Xue. I designed sgRNAs using MIT.CRISPR.edu and by manual review. I synthesized and cloned all sgRNAs. I performed all cell culture, qPCR, western Blot, TIDE and Surveyor Assays. For all preceding experiments I was assisted by Haiwei Mou. For cell culture assays, I was assisted by Suetyan Kwan. The University of Massachusetts Medical School Vector core packaged and performed quality control on AAVs. I performed additional QC. Alexandra Weis performed ICV injections. I performed genotyping, weight, grip strength, neuro-score, and rotarod assays. For all mouse work, I was assisted by Alexandra Weiss and Jake Metterville. Alexandra Weiss and I performed all animal harvests. I performed all tissue sectioning and was assisted by Alexandra Weiss and Jake Metterville. Alexandra Weiss performed ventral root dissections and the UMASS Electron Microscopy core prepared slides for ventral root counts. I performed all Immunofluorescence assays. For neuromuscular junctions, I was assisted by Jake Metterville. For all microscopy, I was assisted by Haiwei Mou, Nick Rice and Samantha Ho. Pin-Tsun Lee performed net axonal transport assays. I performed laser capture microdissections. I was assisted by

Harry Haruhiko and Rachel Stock. Ventral root sectioning and mounting was performed by the UMass Electron Microscopy Core.

4.2 Abstract

Mutations in the *SOD1* gene are the most characterized genetic cause of amyotrophic lateral sclerosis (ALS) and account for ~20% of inherited cases and 1-3% of sporadic cases. The gene-editing tool Cas9 can silence mutant genes that cause disease, but effective delivery of CRISPR-Cas9 to the central nervous system (CNS) remains challenging. Here, I developed a strategy using canonical *Streptococcus pyogenes* Cas9 and guide RNA packaged into separate AAV9 vectors to silence *SOD1* following delivery into the cerebral ventricles. I demonstrate effectiveness of delivering Cas9 to the CNS in a transgenic mouse model. Mice treated with both AAV.Cas9 and AAV9.gRNA had prolonged survival when compared to mice treated with AAV.Cas9 only. Treated mice also had improved grip strength, improved rotarod function, and improved net axonal transport. This study demonstrates that AAV delivery of Cas9 and guide RNA can mediate disease gene silencing of *SOD1* in motor neurons and necessitates further development for use as a therapeutic intervention for *SOD1*-linked ALS patients.

4.3 Introduction

ALS is a neurodegenerative disease in which loss of upper and lower motor neurons results in progressive muscle weakness, paralysis, and death, typically within 2-5 years of onset[121,122]. There is a clear need to develop treatments for ALS; only two FDA-approved drugs are available, with each providing modest delays in ALS progression. Riluzole, a sodium channel blocker approved in 1995, extends patient survival by approximately three months[8]. Edaravone, a novel free-radical scavenger approved in 2017, slowed early-stage ALS progression in a 6-month trial[9]. Currently, the impact of edaravone on patient survival has not been reported.

Approximately 90% of ALS cases are sporadic and 10% of cases are familial[122]. Currently, over 30 genes are associated with familial ALS, Mutations in the free-radical scavenger gene *SOD1* (Cu-Zn superoxide dismutase 1) are the second most common genetic cause of ALS, accounting for ~20% of familial cases and in 1-3% of sporadic cases[13–16]. ALS-associated *SOD1* mutations destabilize the protein, causing aberrant misfolding and aggregation that likely contribute to cell death[16,119]. The mechanism of how SOD1 misfolding causes cell death is not fully understood, but numerous pathways have been implicated—glutamate excitotoxicity, mitochondrial dysfunction, synaptic transport deficiency, and impairment of autophagy and the proteasome[50,71,123–126]. Interestingly, aberrant SOD1 misfolding is also observed in a subset of ALS cases lacking

SOD1 mutations[15,20,32], suggesting that mutant and wtSOD1 may contribute to pathology in a similar manner. Thus, targeting *SOD1* may have therapeutic potential beyond those with a mutant *SOD1* gene.

Numerous studies have demonstrated that repressing SOD1 ameliorates ALS in animal models by delaying onset, and increasing survival[14,23,72–74]. Many of these studies used the *SOD1*^{G93A} (gain-of-function mutation) transgenic mouse model, which exhibits motor neuron loss and a shortened lifespan (5 to 6 months). Previous strategies to repress SOD1 in transgenic animal models include neutralizing antibodies[34], antisense oligonucleotides (ASOs)[75], viral vector-mediated delivery of short hairpin RNA (shRNA)[73,76], artificial microRNA (miR)[72], and chemically-modified shRNA[23]. The wealth of literature describing the outcomes of *SOD1* silencing make the mouse model an excellent candidate for studying the therapeutic potential of CRISPR-based gene editing.

CRISPR-associated Cas9 protein (Cas9) binds with a single guide RNA (sgRNA) to cleave genomic DNA. Cas9 can target anywhere in the genome where there is a Protospacer Adjacent Motif (PAM), a short sequence of 2-6 nucleotides. Cas9 proteins from different species of bacteria recognize different PAMs. After cleavage, the Non-Homologous End Joining (NHEJ) repair pathway can introduce frameshift insertion/deletion mutations, resulting in gene silencing via nonsense-mediated decay[1,91,93].

The CRISPR genome editing system has been demonstrated to work in the brain and spinal cord of mammals[96,97]. In comparison to other methods of gene silencing, A Cas9 strategy for silencing *SOD1* is appealing because of ability to target the genome and cause permanent alteration, eliminating the need for repeat doses, or delivering persisting AAVs, and reducing potentially harmful immunogenic responses.

Recently, *Staphylococcus aureus* Cas9 (saCas9) was used to silence *SOD1* in mice[127]. The small size of saCas9 is advantageous for *in vivo* delivery, yet it recognizes a long “NNGRRT” PAM that limits the number of available PAMs in the genomic region of interest. By contrast, *Streptococcus pyogenes* Cas9 (SpCas9) recognizes a short “NGG” PAM that enables a larger selection of target sites in the gene of interest. Developing an *in vivo* delivery platform for SpCas9 will expand the genome editing toolkit for studying ALS.

Adeno-associated virus (AAV) is the favored delivery vector for gene therapies due to its low pathogenicity and ability to infect nondividing cells, including motor neurons[31]. However, the cargo size of AAVs is small, and co-expressing the large SpCas9 (4.3kb), sgRNA and requisite regulatory elements in the same AAV vector is challenging. In this study, we applied a dual vector strategy in which SpCas9 and sgRNA are on separate AAV9 vectors. We demonstrate that this delivery platform can target *SOD1* in brain and spinal tissue and prolong survival in the *SOD1*^{G93A} mouse model of ALS.

4.4 Results

4.4.1 Design and Screening of sgRNAs and *in vitro* validation

We designed sgRNAs within the first three exons of the human *SOD1* locus (Fig. 9A top panel) and cloned them into separate lentiV2 plasmids. To test sgRNA silencing efficacy, we generated stable cells using the diploid human HCT116 cell line for each sgRNA and measured SOD1 protein levels by Western Blot (Fig. 9B). Our top sgRNA candidate, guide E2C (hereafter called sgSOD1) had the highest knockdown efficiency (Fig. 9B), and targeted both wildtype and G93A human *SOD1* alleles. To determine if knockdown was due to the generation of indels near the target site of sgRNA, we sequenced the sgRNA target region and detected indels at the predicted location (Fig. 9C). We further confirmed *SOD1* mRNA knockdown using qPCR (Fig. 9D). To ensure that the efficiency of sgSOD1 was not specific to one cell line, we transiently infected two additional cell lines—human embryonic kidney HEK293T and human neuroblastoma SH-SY5Y—with AAV9 plasmids (described in next paragraph) and detected indels at the predicted location (Fig. 9E).

b

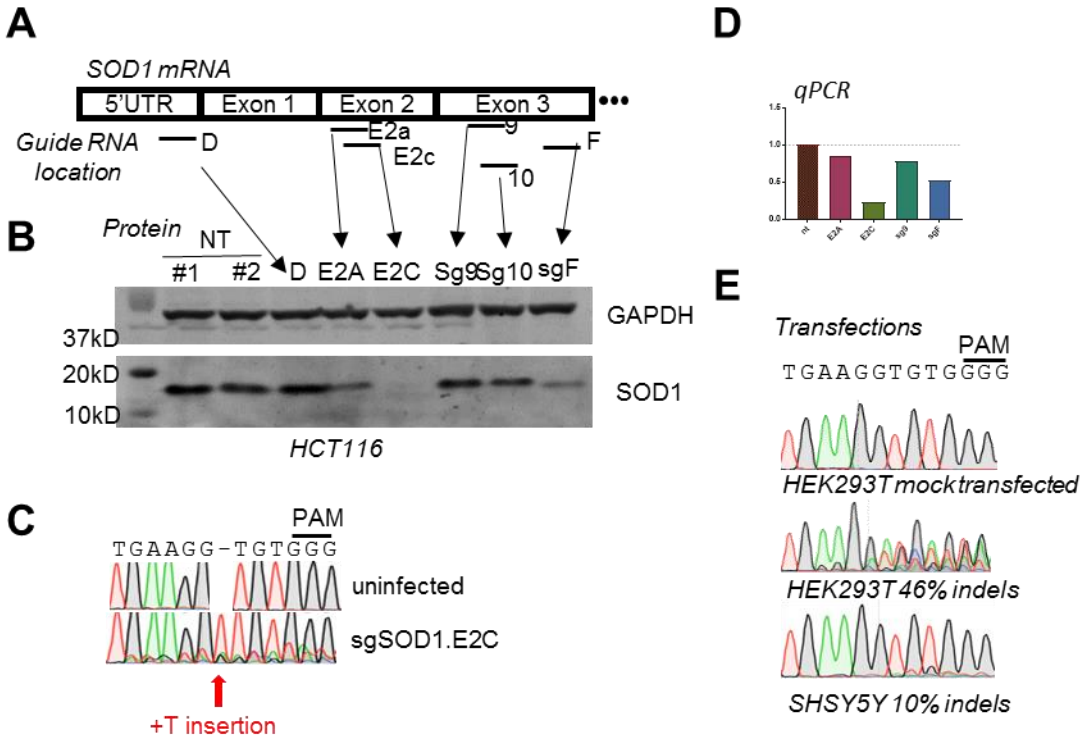

Figure 9. *in vitro* CRISPR-mediated editing of human *SOD1*

(a) Map of gRNAS against *SOD1* in screen **(b)** Protein analysis via western blot. sgSOD1 depletes SOD1 in HCT116 cells stably expressing Cas9 and sgRNAs. GAPDH serves as a loading control **(c)** Indel formation of sgRNA E2C in HCT116 stable cell line HEK293T. sgE2C, hereafter called sgSOD1, was selected for further characterization **(d)** qPCR of *SOD1* in HCT116 stable cell lines (e) Sequencing traces in various cell types 72 hours after infection with AAVs expressing Cas9 and sgSOD1. **(e)** Sequencing traces of DNA from various cell lines 72 hours after infection with AAVs expressing Cas9 and sgSOD1.

4.4.2 AAV Packaging and AAV9 selection

sgSOD1 targeted *SOD1* within the second exon and utilized a GGG PAM (Fig 10A). For *in vivo* experiments, we generated two AAVs, one expressing

Cas9 (a gift from the Gao lab) and the other expressing sgSOD1 (backbone addgene # 60958). We choose the AAV9 capsid because of its well-established ability to infect motor neurons[76]. The AAV9.sgSOD1 comprises a U6 promoter driving sgSOD1 and a hSYN1 promoter driving an EGFP-KASH protein, which localizes GFP to the outer nuclear membrane. AAV9.Cas9 comprises a pU1A promoter driving HA-NLS-Cas9-NLS (Fig. 10B).

To confirm whether our AAV9 vectors containing Cas9 and sgSOD1 could silence *SOD1* expression *in vitro*, we infected HEK293T cells with AAV9.sgSOD1 and AAV9.Cas9 and measured SOD1 protein levels. We detected a significant decrease in SOD1 protein at 72 hours post infection (Fig. 10C).

4.4.2 Survival and behavior

To determine if we could edit *SOD1 in vivo*, we delivered our dual AAV9 system to transgenic *SOD1*^{G93A} mouse pups (postnatal day 1, or p1) via intracerebroventricular (ICV) injections (hereafter referred to as sg*SOD1* mice, n=38) (Fig. 10D). While previous studies have used facial vein injections to deliver AAV9 to the CNS, including our own work, we chose ICV injections based on their ability to distribute throughout the CNS. Moreover, ICV uses less volume and targets fewer non-CNS tissues than facial vein injection[72], limiting off-tissue expression of Cas9 outside of CNS. For controls, we used 3 groups: (1) un-injected *SOD1*^{G93A} mice (n=13), (2) mice with AAV9.Cas9 only (n=14), and (3) mice with AAV9.Cas9 and AAV9 containing a non-targeting sgRNA (hereafter

referred to as sgControl mice) (n=13). We then monitored all mice throughout their lifespan for motor symptoms.

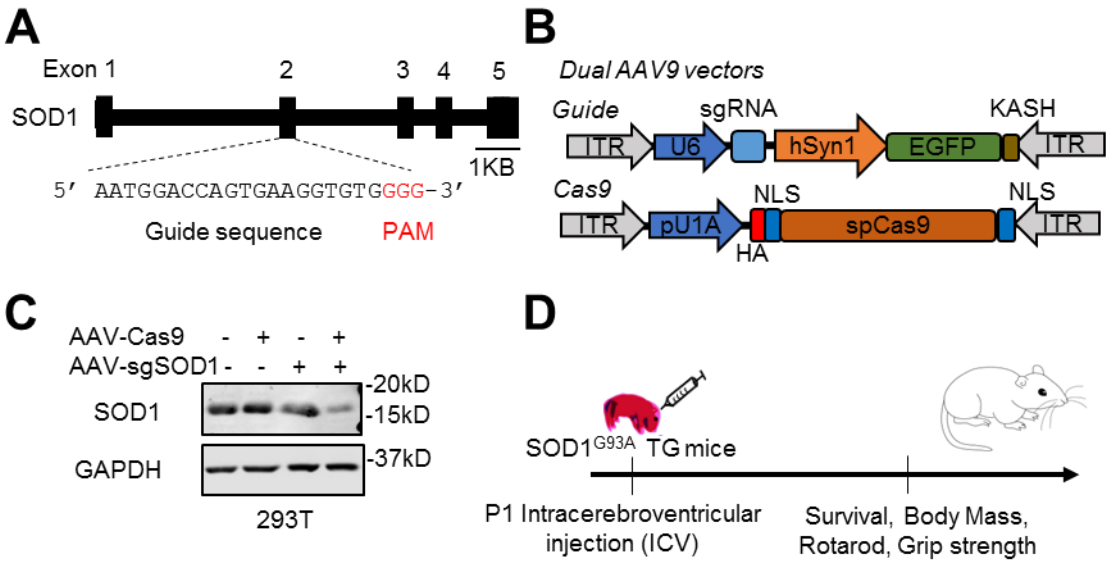

Figure 10. *in vivo* CRISPR-mediated editing of human *SOD1*

(a) sgSOD1 targets the second exon of human SOD1. **(b)** Schematic of dual AAV9 vectors used for in vivo experiments. For the guide AAV9, a U6 Pol III promoter drives sgRNA and the human Synapsin promoter drives EGFP-KASH expression. The KASH domain localizes GFP to the nuclear membrane. For the Cas9 AAV9 vector, the ubiquitous pU1A promoter drives the spCas9, which contains a 5' HA Tag and flanking NLS signals. **(c)** sgSOD1 depletes SOD1 protein in HEK293T cells 72 hours after infection with AAV9.sgSOD1. GAPDH serves as a loading control. **(d)** Schematic of in vivo experiment design. SOD1G93A transgenic mice (p1) received 2ul each undiluted AAV vector delivered bilaterally into the cerebral ventricles.

We compared survival of mouse groups using Kaplan Meir graphs. Compared to all control groups, AAV9 sgSOD1 mice had increased survival (median survival 154 vs 134 days of sgControl+Cas9, $p<0.0001$) (Fig. 11A-B).

There was no significant difference in survival amongst control groups (sgControl+Cas9 vs Cas9 only, p =0.99; sgControl + Cas9 vs uninjected, p=0.17). sgSOD1+Cas9 mice also had a significant delay in disease onset, as measured by peak body weight (Fig. 11C-D, 115 days vs 99 days of sgControl+Cas9 mice, p<0.001).

Extending disease duration, (i.e., increasing time between disease onset and endpoint of a mouse) is an important metric with regards to clinical application, as any therapeutic that could work after onset of symptoms would be favorable. Thus, we sought to determine if there were any changes in disease duration between sgControl and sgSOD1 mice. In the aforementioned survival graphs, the delay in onset was approximately equal to the increase in survival, suggesting that the duration of disease is not affected by *SOD1* silencing. Furthermore, we found no correlation between duration of disease and survival in either sgSOD1, sgControl, or Cas9 only mice (Fig. 12C). Finally, to account for the possibility of AAV transduction variation affecting disease duration (i.e., mice receiving different doses due to human error), we compared median disease duration between high-surviving sgSOD1 mice (i.e., mice with survival 150 days or longer) vs sgControl (Fig 12D. There no significant difference between these groups (Fig. 12C, 39.4 days vs 36.08, p-value 0.556).

sgSOD1 mice showed significant improvement in grip strength starting at week 15 and rotarod performance starting at week 18 compared to sgControl

and Cas9 only mice (Fig. 11E and Fig. 12A). sgSOD1 mice also showed significant improvement in rotarod performance (Fig. 11F and Fig. 12B).

To ensure that sgSOD1 treated mice had no other adverse or unexpected symptoms, we monitored all mice for any changes in behavior, or health issues. Across all control groups, we observed six unexpected and adverse events that include bloated abdomen, obesity, death of mouse not due to paralysis, eye infection, hyperactivity, kyphosis, or seizures (Table 3).

	sgSOD1 *n=38*		**sgControl** *n=14*		**Cas9 only** *n=16*	
Unexpected/adverse event	**m** *n=22*	**f** *n=23*	**m** *n=7*	**f** n=7	**m** *n=8*	**f** *n=8*
bloated abdomen	2 (9.1%)	-	-	1 (14%)	-	1 (12.5%)
obese	2 (9.1%)	-	-	-	-	1 (12.5%)
died not at endpoint	4 (18.1%)	-	1 (14%)	-	4 (50%)	-
eye infection	4 (18.1%)	-	-	-	-	-
hyperactive	1 (4.5%)	-	-	-	-	-
kyphosis	2 (9.1%)	1 (4.3%)	-	-	-	1 (12.5%)
seizure or immobile	2 (9.1%)	-	-	1 (14%)	-	-

Table 3. Unexpected and adverse events in mice

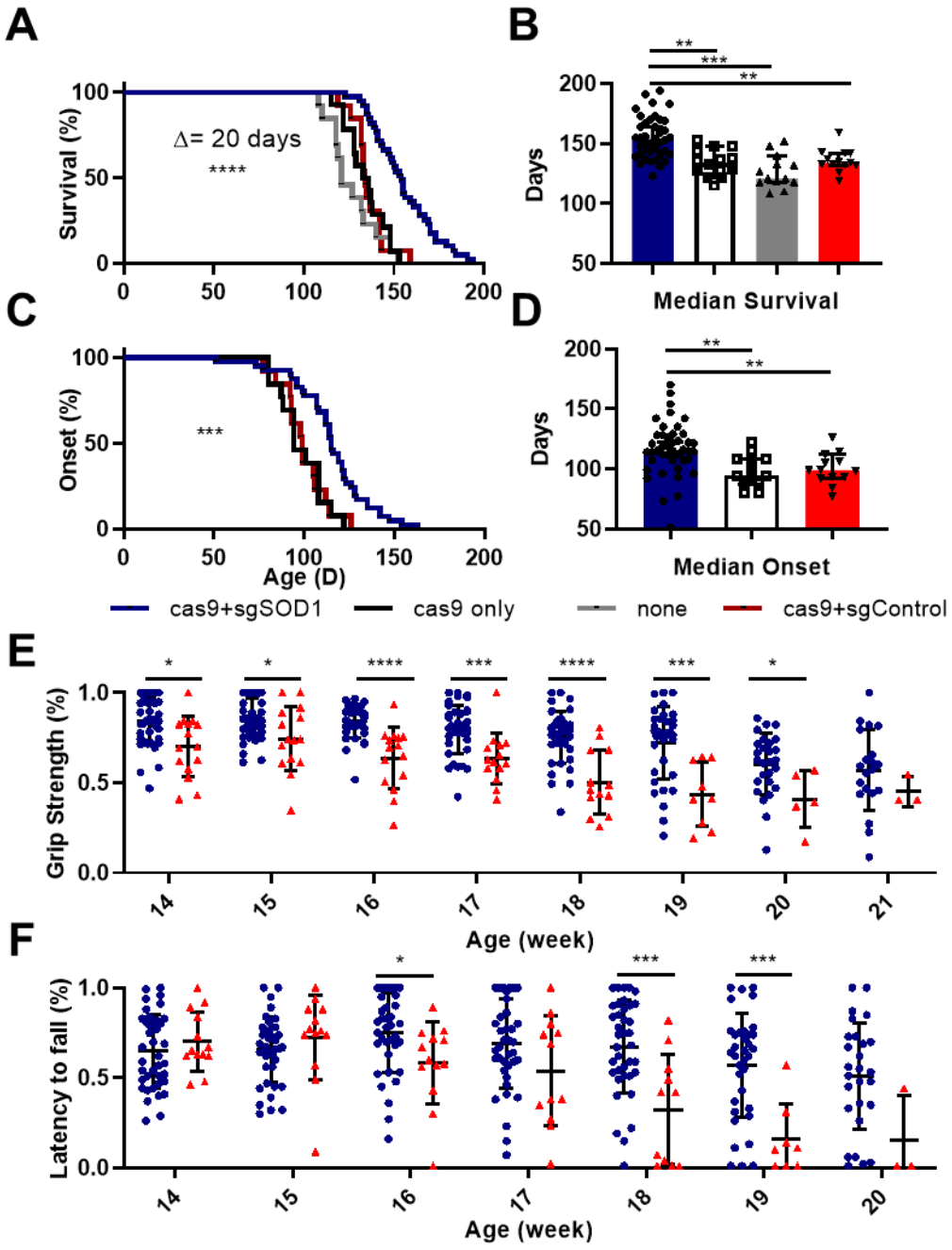

Figure 11. AAV CRISPR treatment prolongs survival in *SOD1^{G93A}* mice.

SOD1^{G93A} mice were monitored daily by a blinded observer until they reached experimental endpoint. Mice were either untreated (n=14), sgSOD1 (n=38), sgControl (n=13), or Cas9 only (n=13). **(a-b)**. Median survival is 154 days for sgSOD1 and 134 days sgControl (p<0.0001). Error

bars on panel B show median and 95% confidence interval. **(c-d)** Median disease onset is 115 days for sgSOD1 and 99 days for sgControl p<0.001. Error bars on panel B show median and 95% confidence interval. (e) Grip strengths for all four limbs per mouse were normalized. Significant differences between sgSOD1 and sgControl were first detected at week 14. **(f)** Rotarod performance of sgSOD1 and sgControl mice were assessed by rotarod performance. Significant differences were first detected at week 16. For panels E and F, error bars represent standard deviation. *p<0.05, **p<0.01, ***p<0.001, ****P<0.0001.

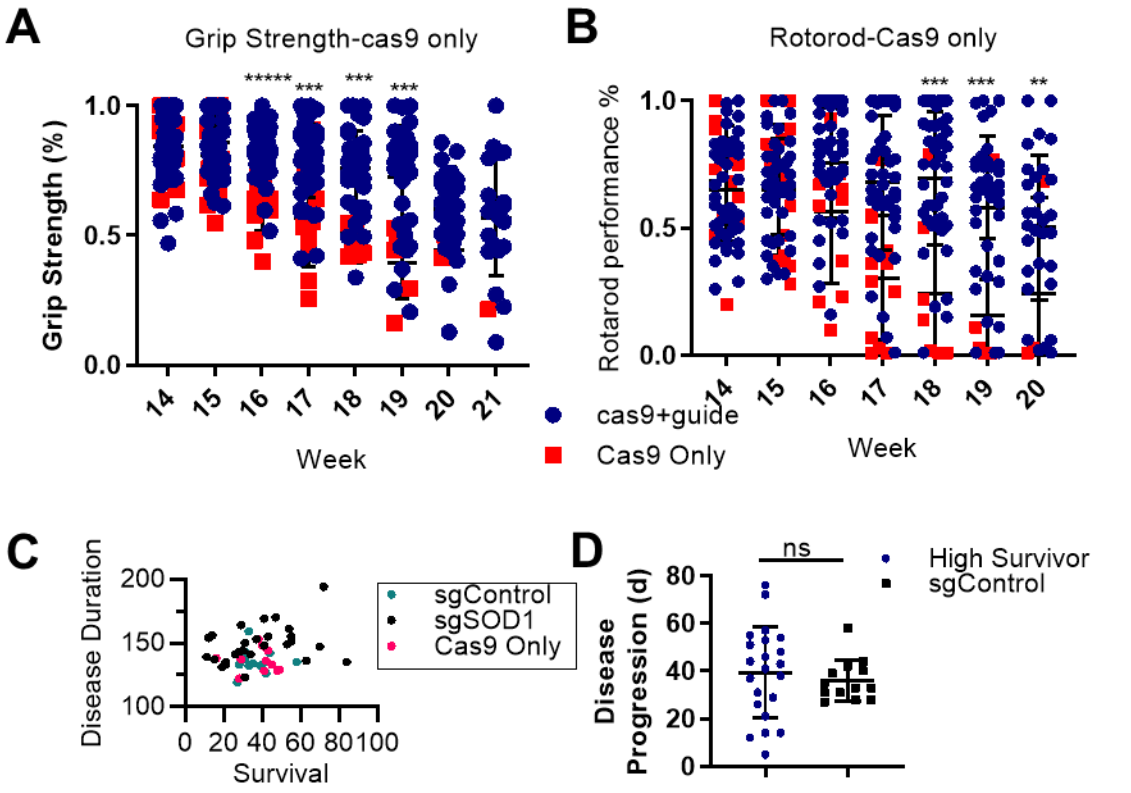

Figure 12. AAV CRISPR treatment delays motor symptoms and duration of disease.
(a) Grip strengths from all four limbs per mouse were normalized. Significant differences between sgSOD1 and Cas9 only groups were first detected at week 16. **(b)** Rotarod performance of sgSOD1 mice. Significant differences were first detected at week 17. **(c)** Disease duration sgSOD1 mice, and sgControl mice and Cas9 only mice. Pearson correlation coefficients = 0.12 for sgSOD1, >0.01 for sgControl, and 0.01 for Cas9 only **(d)** disease progression vs age of onset in high survivor sgSOD1 and sgControl mice, Fischer r to z test, z=0.41, not significant. Error bars represent standard deviation. *p<0.05, **p<0.01, ***p<0.001, ****P<0.0001.

4.4.3 Tissue distribution and indel formation in brain and spinal cord tissue

To determine if our dual delivery injection of AAV9.sgSOD1 and AAV9.Cas9 was efficiently distributed throughout the CNS, we immunoassayed brain and thoracic spinal cord sections for GFP (used as a marker of AAV9.sgSOD1) and HA-tagged Cas9. (Fig. 13A and 13B, respectively). We detected both AAV9 vectors in the brain and the thoracic spinal cord.

To confirm signal detection of the AAV9.sgRNA vector, we observed slides of spinal cord using confocal microscopy for GFP signal (Fig. 13C). GFP-KASH was found to localize to the outer membrane of the nucleus, as expected. To confirm signal detection of the AAV9.Cas9 marker, we immunoassayed with another antibody, anti-Cas9, and observed signal in the spinal cord (Fig. D).

To determine if the Cas9 and sgSOD1 generated indels at the *SOD1* locus, we targeted deep sequencing of the *SOD1* locus in the brain and lumbar spinal cord and analyzed sequencing using CRISPRESSO[117]. We found indels at the targeted locus with an average editing frequency of 4.181% in the cortex and 0.4% in the lumbar spinal cord. (Table 4). The results were similar to the *in vitro* results, the most prominent indel detected was the insertion of a thymine three nucleotides upstream of PAM (Fig. 14).

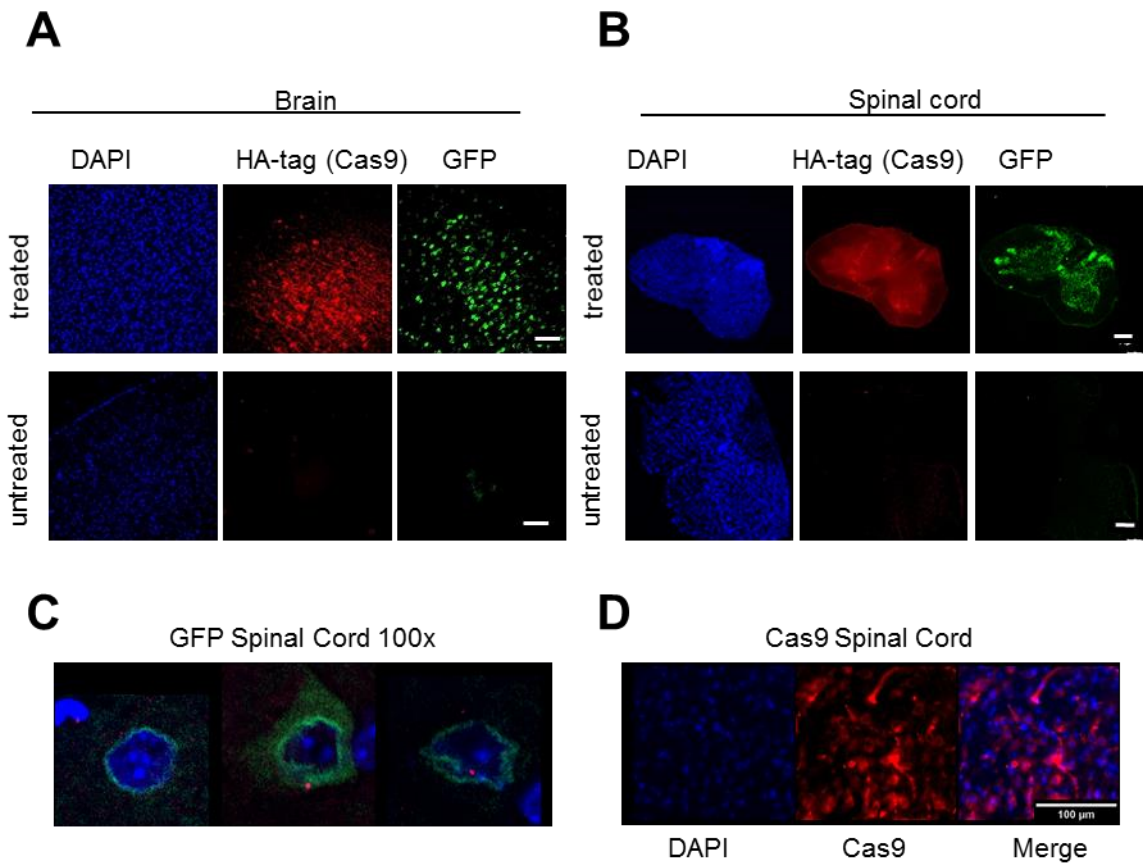

Figure 13. Distribution and detection of AAV vectors in CNS

(a-b) Detection of GFP and Cas9 in the cortex (a) and spinal cord (b) of sgSOD1 mice. Native GFP detection. For detection of Cas9, anti-HA antibodies were used. Scale bar 100µm. **(c)** Confocal image of GFP localized to nuclear membrane, 100x magnification **(d)** Detection of Cas9 using Cas9 antibodies in the spinal cord, scale bar 100µm.

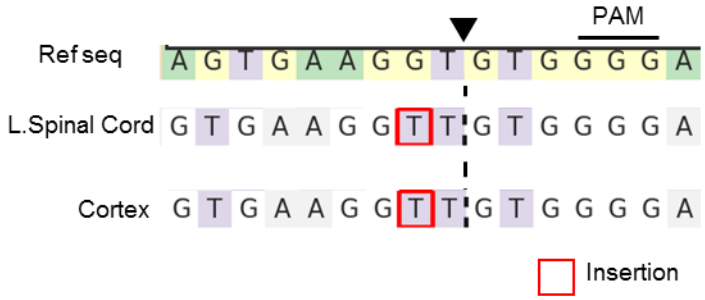

Figure 14. Indels generated by sgSOD1

Representative sequence traces of Indels dected by CRISPRESSO located at the predicted targeted locus with SOD1 from Lumbar spinal cord and Cortex.

Tissue	*Treatment*	*avg indel %*	*Fold change*	*Coverage Range (#reads)*		
Cortex	control	0.077	54x	2,129,209	-	3,015,574
	sgSOD1	4.181		583,546	-	3,234,125
LSC	control	0.041	10x	281,203	-	2,584,891
	sgSOD1	0.404		502,527	-	2,235,998
Liver	control	0.034	54x	331,566	-	576,528
	sgSOD1	1.865		2,534,548	-	3,018,736

Table 4. Deep sequencing of sgSOD1 locus in the CNS and liver

4.4.4 Preservation of structure of distal axonal processes

Neuromuscular junction destruction and distal axonal pathology are hallmarks of neuro-degeneration in *SOD1*^{G93A} mice[128–130]. To determine if increased survival was due, in part, to preserved distal axonal architecture, we analyzed neuromuscular structures of mice at disease midpoint (p110). We stained fixed gastrocnemius muscle with antibodies against presynaptic motor

neuron markers—βIII tubulin and synaptophysin—and with α-bungarotoxin, which binds to acetylcholine receptors in the post-junctional folds of the muscle. We compared the number of intact, partially intact, and denervated neuromuscular junctions (Fig. 15A). Compared to sgControl, sgSOD1+Cas9 mice had significantly more intact neuromuscular junctions (87.3% ± 6.2% vs 49.7% ± 10.8%, $p<0.01$) (Fig. 15B). Conversely, sgSOD1+Cas9 mice had significantly less partially intact (7.3% ± 4% vs 27.4% ± 3.3%, $p<0.01$) and denervated (5.3 ± 2.4 vs 29.6 ± 3.1%, $p<0.001$) neuromuscular junctions compared to sgControl. The number of intact, partially intact, or denervated junctions were similar between sgSOD1+Cas9 and wt littermate controls (Fig. 15B, intact: 87.3% ± 6.2% vs 94.3% ± 2.4%; partially intact: 7.3% ± 4.0% vs 4.8% ± 2.2%; denervated: 5.3% ± 1.4% vs 1.4% ± 0.8%, respectively).

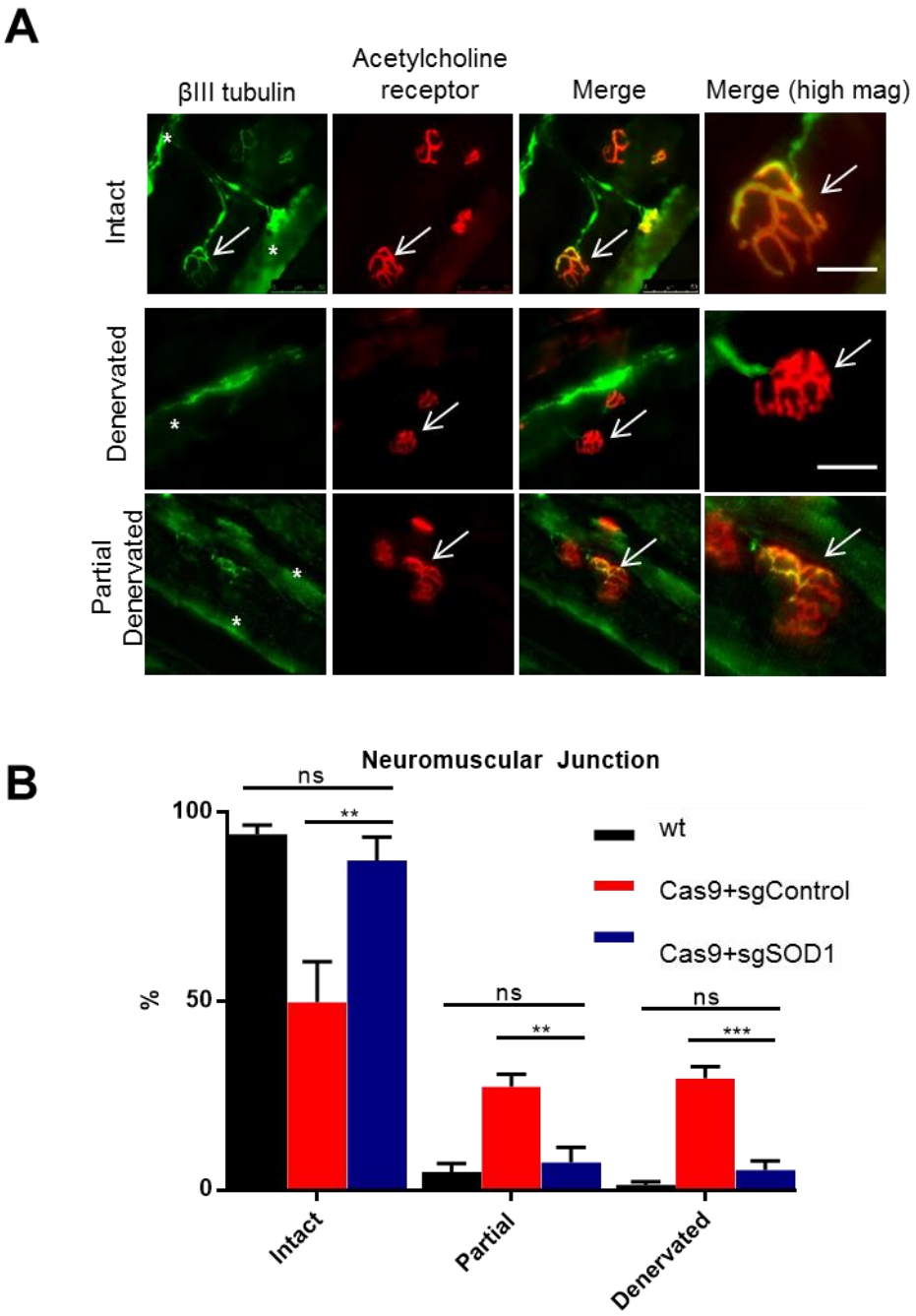

Figure 15. sgSOD1 treatment preserves neuromuscular junction structure.

(a) sgSOD1 mice were sacrificed at disease midpoint (p110). Gastrocnemius muscles were immunostained for the neuromuscular markers anti-synapsin and anti-βIII tubulin (shown here as green), and for the postsynaptic muscle fiber marker acetylcholine receptor using α-bungarotoxin (shown here as red). Representative images of intact (upper panel), partial denervated (middle panel), and denervated (lower panel) neuromuscular junction. Arrows denote neuromuscular junctions. * denotes autofluorescence of muscle fibers. **(b)** Quantitation of percentage of intact, partially intact and fully-denervated NMJs. Error bars are standard deviation, ** $p<0.01$, ***$p<0.001$. n=3 mice (>300 NMJs per mouse).

4.4.5 Preservation of structure of proximal axonal processes

To determine if sgSOD1 could preserve proximal axonal architecture, we sectioned the ventral root from the L5 lumbar region and observed axon cross sections via microscopy (Fig. 16A). We plotted ventral root axon diameters from mice sacked at disease midpoint (p110) mice in a histogram binned by size. The resulting histograms for all mouse groups showed a characteristic biphasic distribution of both axons per section and counts of, with large-diameter axons comprising α motor neurons and small diameter axons comprising gamma-motor neurons. The large diameter, α-motor neurons generate force and are susceptible to degeneration during ALS while the small diameter, gamma-motor neurons provide proprioceptive feedback to α-motor neurons and are usually spared of degeneration in ALS models[131]. sgSOD1 mice had significantly more intact motor neuron axons measured by frequency distributions of axon diameters (Fig. 16B showing histogram of axon diameter, and Fig.16C showing histogram of large axon diameter counts). These data indicate that CRISPR

treatment preserved the architecture of motor neuron and neuromuscular junctions.

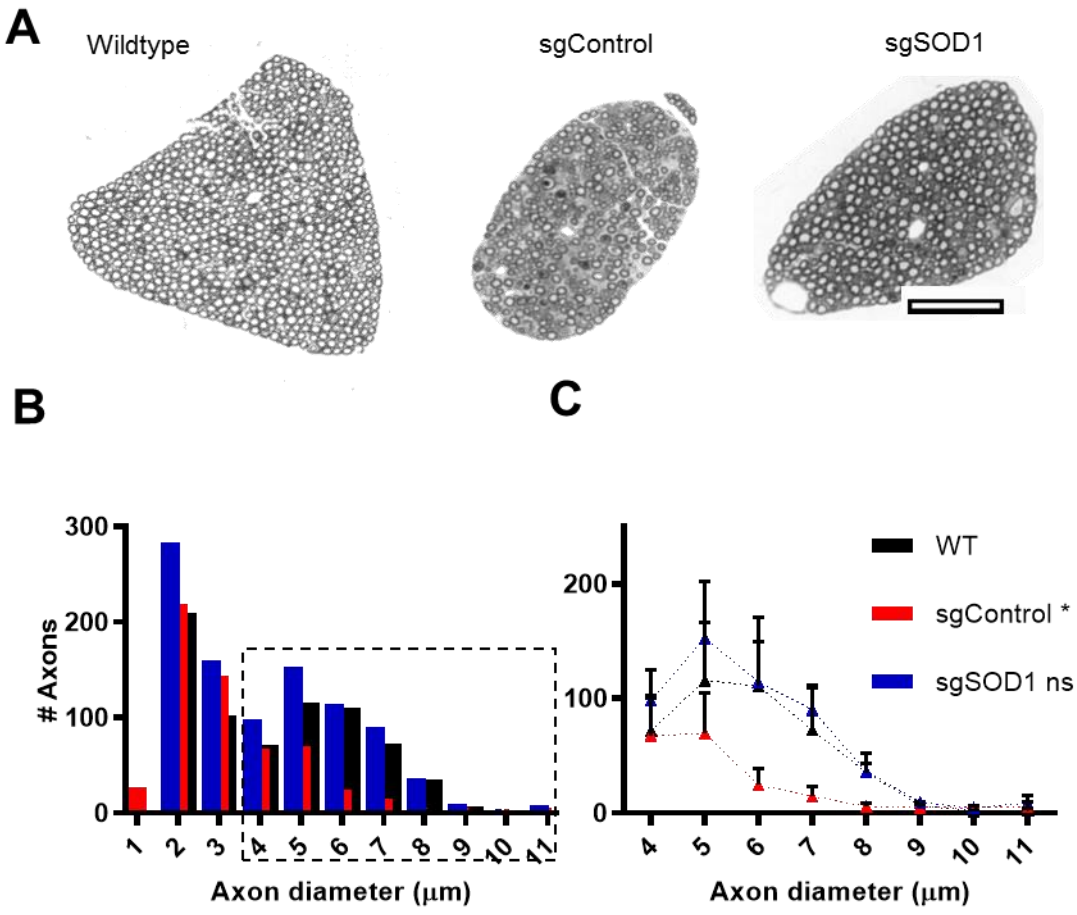

Figure 16. sgSOD1 treatment delays motor neuron axonal degeneration in mice of disease midpoint (p110) mice.

(a) Representative images of cross sections of ventral nerve root from the the L5 lumbar spinal segment from wildtype, sgSOD1 and sgControl mice. Scale bar for top panel: 100μm. **(b)** Frequency distribution of axon diameters amongst three groups. **(c)** Inset of motor neuorons (axons diamter greater than 4μm), p-value from one way ANOVA of sgSOD1 and sgControl with pairwise comparison to wt mice. p=0.044 for sgControl and p- = 0.271 for sgSOD1. Error bars denote s.e.m.

4.4.6 Preservation of function of axon transport in lower motor neurons

To determine if the observed preservation of axon architecture confers a functional improvement, we measured net axonal transport in live mice using an assay developed by Pin-Tsung Lee and Robert Brown. The assay quantifies uptake of ^{125}Iodine conjugated C-terminal portion of the Tetanus Toxin (TTC) that binds to the presynaptic membrane of the neuromuscular junction and is internalized and transported in a retrograde fashion to the spinal cord[132]. Following injection of ^{125}Iodine conjugated TTC into the tibialis anterior muscle, uptake of the TTC into the corresponding L4-L5 motor neurons is quantified using single photon emission computed tomography (SPECT).

We injected TTC into the tibialis anterior muscles of live mice at an early onset time point (p85) and a mid-disease time point (p110) and measured TTC uptake into the spinal cord. (Fig. 17A and 17B). For controls, we used *SOD1*^{G93A} untreated mice. At p85, the uptake of TTC in sgSOD1 mice was similar that of wt littermates and significantly higher than that of untreated *SOD1*^{G93A} mice. At p110, sgSOD1 mice showed significant increased TTC uptake as compared to untreated *SOD1*^{G93A} mice at day 85 (Fig. 17C). These data suggest that CRISPR treatment improved net axonal transport. Moreover, net axonal transport detected benefit of *SOD1* silencing at 85 days, well before any other outcome measured (e.g., grip strength, 112 days, rotarod 119 days).

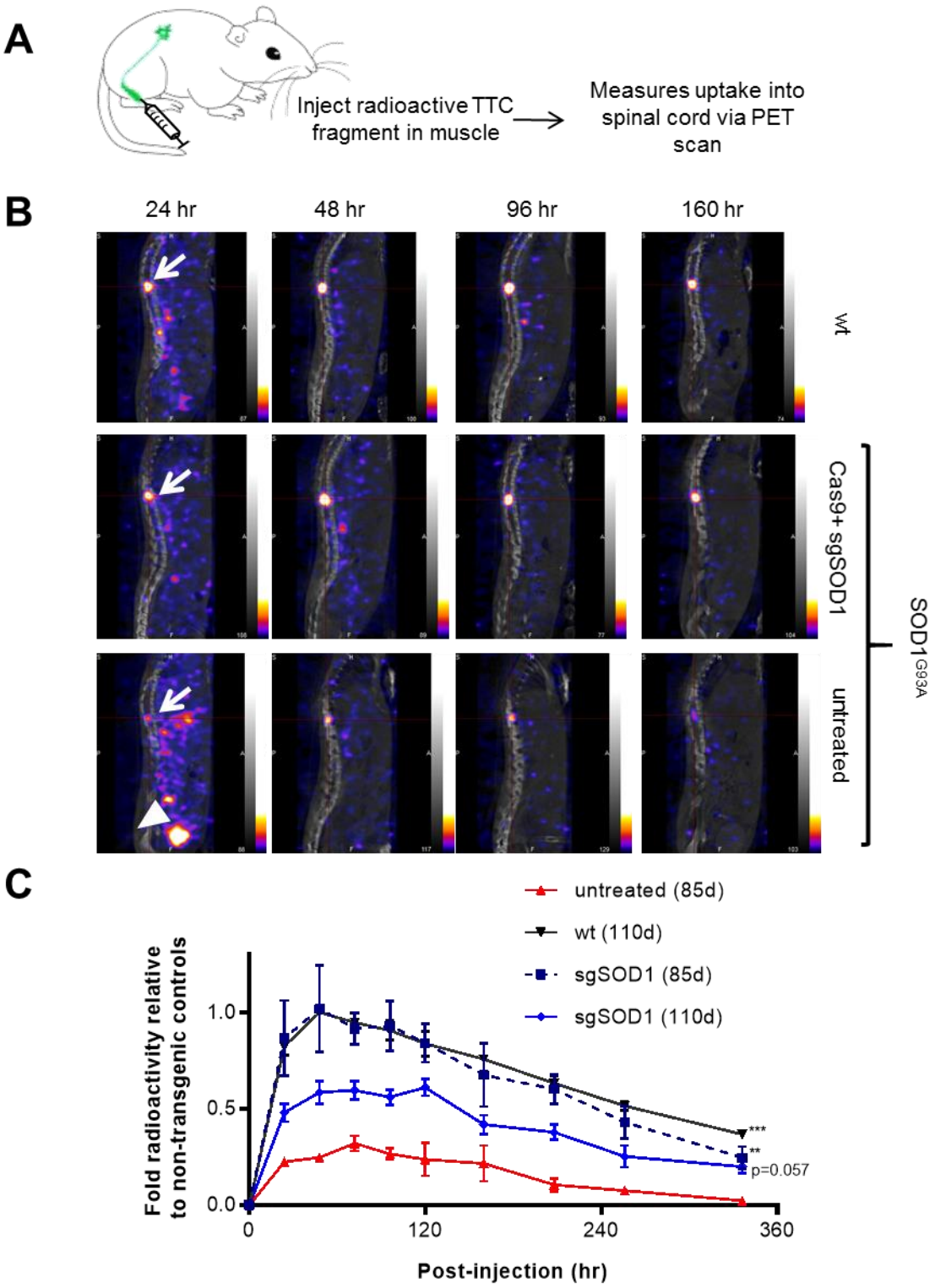
A
Inject radioactive TTC fragment in muscle
Measures uptake into spinal cord via PET scan
B
24 hr
48 hr
96 hr
160 hr
wt
Cas9+ sgSOD1
untreated
SOD1G93A
C
untreated (85d)
wt (110d)
sgSOD1 (85d)
sgSOD1 (110d)
Fold radioactivity relative to non-transgenic controls
1.0
0.5
0.0
0
120
240
360
Post-injection (hr)
***
**
p=0.057

Figure 17. AAV CRISPR treatment improves net axonal transport in mice.

(a). Measurement of net axonal transport using tetanus toxin fragment C (TTC). TTC was injected in the tibialis anterior muscle of wt. untreated, sgSOD1, and untreated *SOD1*^{G93A} mice and mice were imaged using SPECT at pre-disease (p85) and disease midpoint (p110) timepoints. **(b)**. Representative PET scan images. Arrows denote radioactivity in spinal cord. Triangle denotes site of injection. **(c)** Radioactivity vs time plots of TTC signal in the spinal cord. Error bars represent S.E.M. 2-way ANOVA multiple comparisons with pairwise comparison to wt untreated mice, $**p<0.01$, $***p<0.001$.

4.4.7 Decrease in SOD1 protein detected in brain and in motor neurons within spinal cord

To determine whether the sgSOD1 treatment reduces SOD1 proteins in the spinal cord, we performed an ELISA assay from whole cortical and lumbar spinal tissues. Given our sequencing data showed higher percentages of indels in the cortex than in the spinal cord, we hypothesized that there would be more SOD1 knockdown in the brain compared to the spinal cord. In the brain, when compared to sgControl mice, sg SOD1 mice had 60% reduction in SOD1 protein (Fig. 18A left panel, 2.9 vs 9.2ng/ml, p=0.033). Intriguingly, there was no difference in SOD1 protein in the lumbar spinal cord (Fig. 18A, middle panel, p=0.845). We also observed a 60% reduction of SOD1 in the liver (Fig. 18A, right panel, 3.8 vs 9.8 ng/ml, p=0.013).

The lack of SOD1 decrease in the spinal cord was surprising, since we had measured improvements in axon structure and function. We hypothesized that SOD1 may be specifically downregulated in motor neurons, but not in other

cell types, which could explain the lack of significant downregulation of SOD1 from whole lumbar spinal cord tissue. To this effect, we performed laser-capture microdissection of motor neurons in the lumbar spinal cord and assessed protein levels by gel capillary western blotting (ProteinSimple) (See Fig. 18B for representative images of captured tissue). We captured precisely 150 motor neurons per mouse and assayed SOD1 levels. We found a ~50% decrease in SOD1 protein when compared to controls (Fig. 18C shows gel image and Fig 18D shows quantitation of SOD1, p-value = 0.01), suggesting silencing of SOD1 is selective to in motor neurons.

The gel capillary western blot results revealed the presence of SOD1 immunoreactive bands at 44 and 62 kilodaltons. These molecular weight of these immunoreactive bands correspond with the predicted SOD1 molecular weight of SOD1 dimers and trimers, suggesting that they represent dimerized and trimerized SOD1. Since trimeric SOD1 is cytotoxic[37,133], we measured abundance of the putative SOD1 trimeric band. When compared to sgControl mice, the SOD1 trimeric band is decreased (Fig. 18E, p-value 0.087), suggesting that sgSOD1 treatment reduces toxic oligomeric forms of SOD1.

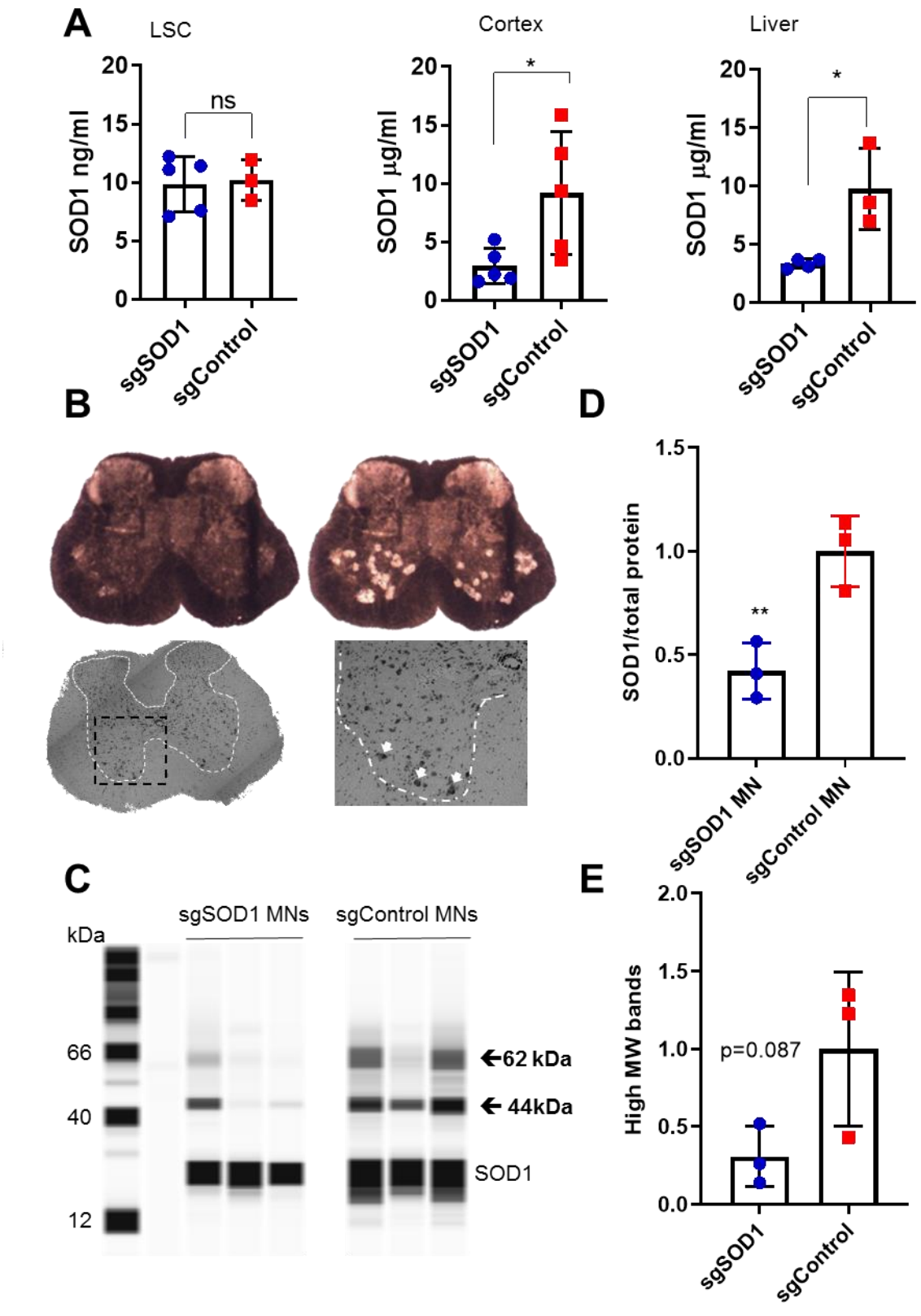
A
LSC
Cortex
Liver
SOD1 ng/ml
SOD1 µg/ml
SOD1 µg/ml
ns
*
*
20
15
10
5
0
sgSOD1
sgControl
B
D
SOD1/total protein
1.5
1.0
0.5
0.0
**
sgSOD1 MN
sgControl MN
C
sgSOD1 MNs
sgControl MNs
kDa
66
40
12
62 kDa
44kDa
SOD1
E
High MW bands
2.0
1.5
1.0
0.5
0.0
p=0.087
sgSOD1
sgControl

Figure 18. SOD1 silencing in the CNS

(a). ELISA assays measuring SOD1 levels in sgSOD1 and sgControl+Cas9 treated mice, n=3-5 per group. Average SOD1 expression from 150 motor neurons in sgSOD1 and sgControl mice was 9.8 vs 10.2ng/ml for LSC p=0.85, 2.9 vs 9.2ng/ml in cortex, p=.03, and 3.35 vs 9.77ng/ml in liver p=0.012. Error bars denote standard deviation. **(b)** Representative images of spinal cord sections before laser capture (top left) and after laser capture (bottom left). Samples, stained, with cresyl violet and cleared with xylene show motor neurons in the ventral horn (top right panel, inset bottom right panel. arrows denote motor neurons. **(c)** Image of gel capillary western blot gel of SOD1. Denoted are SOD1 band at ~25kDa, and two SOD1 immunopositive higher weight molecular bands spaced ~19kDa apart, putatively dimeric and trimeric forms of SOD1. **(d)** Quantitiation of image density of SOD1 bands from gel capillary western blot. Average SOD1 expression in sgSOD1 and sgControl motor neurons was decreased 58%, p-value =0.01. **(e).** Quantitation of image density of putative SOD1 trimeric 62kDA band from sgSOD1 and sgControl mice. Average density of bands show a trend for decreased bands in sgSOD1 mice p-value =0.087. Error bars denote standard deviation.

Both microgliosis and astrogliosis are hallmarks of ALS. To determine whether SOD1 knockdown decreased both types of gliosis, we performed Branched DNA assays (BDNA), targeting the microglial marker IBA1 and the astrocyte marker GFAP of endpoint tissue (Figs. 19A and 19B) We did not find significant differences in either marker among sgSOD1 and sgControl mice in endpoint tissue.

To ascertain whether sgSOD1 silenced mouse endogenous *Sod1*, we performed BDNA assays targeting mouse *Sod1* (Fig. 19C) in tissue at endpoint. We did not find significant differences in mouse *Sod1* between sgSOD1 and sgControl groups. To determine whether sgSOD1 treatment reduced gliosis, we performed BDNA assays on endpoint tissue using markers for reactive

astrocytes, *GFAP*, and microglia, *IBA1*. We found no significant differences in expression of either *GFAP* or *IBA1* [133].

The observation of ~1% gene indel editing and ~50% protein knockdown was unexpected. To further understand the disparity between the efficiency of indel editing and the efficiency of protein knockdown, we looked at mRNA levels of SOD1. Surprisingly, we saw no differences in spinal cord motor neuron SOD1 levels between sgSOD1 mice and control mice, (i.e., non-treated and sgControl mice) (Fig. 20). Furthermore, there was no detectable difference in SOD1 mRNA levels between motor neurons and dorsal horn tissue.

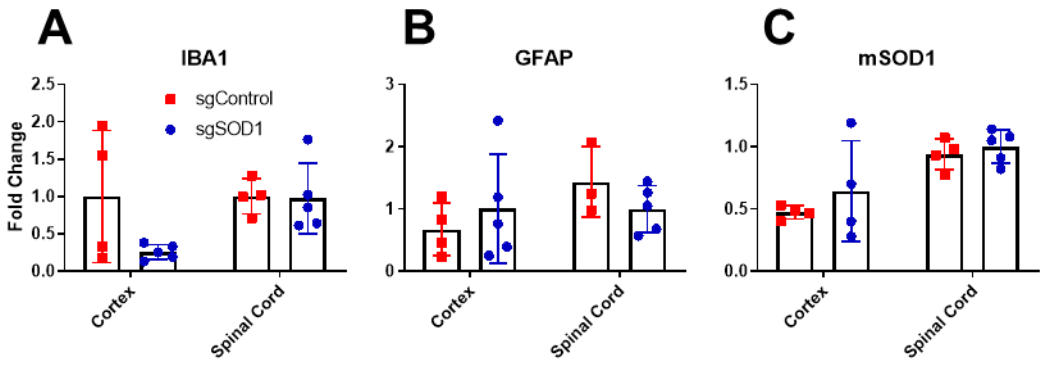

Figure 19. sgSOD1, gliosis and mouse endogenous expression

Branched DNA assays from mouse endpoint tissue **(a)** BDNA assays measuring microglia marker IBA1 in the cortex and spinal cord. **(b)** BDNA assay measuring astrocyte marker GFAP in the cortex and spinal cord. **(c)** BDNA assay measuring mouse *SOD1* in the cortex and spinal cord. Error bars denote standard deviation.

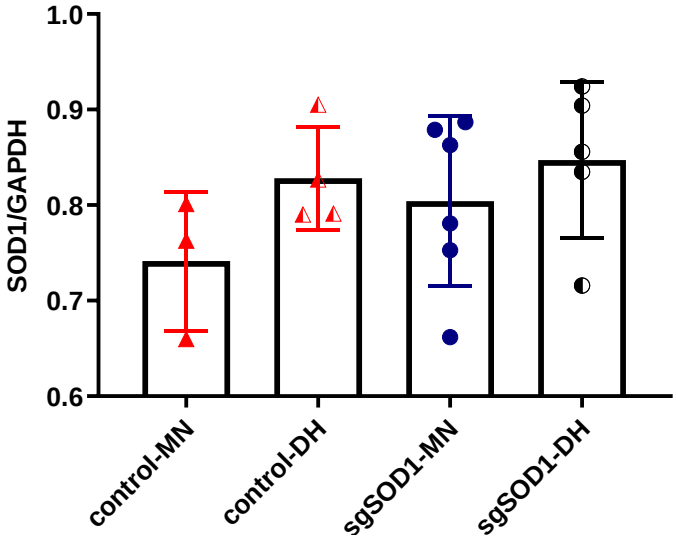

Figure 20. *SOD1* mRNA from motor neurons in spinal cord.

ddPCR following laser capture microdissection of motor neurons (MNs) in the spinal cord. Tissue from the dorsal horn (DH) served as internal controls. Control group comprises both untreated and sgControl mice sgSOD1 mice were treated with sgSOD1 and Cas9. No significant difference between any of the groups observed.

Chapter V Discussion

5.1 Systemic delivery of sgSOD1 prolongs survival in SOD1^{G93A} x Cas9 mice

Here we utilized systemic delivery of AAV9 containing sgSOD1 via facial vein and demonstrated a prolongation of survival and improvement of symptoms in a *SOD1* Cas9 transgenic mouse model of ALS. We detected indel mutations at the predicted locus within *SOD1* at a rate of ~5% in the Brain and 3% in the spinal cord.

While our studies show feasibility of utilizing Cas9 to target *SOD1* in the CNS, several experimental considerations need to be addressed. In these experiments, we used a transgenic mouse model with endogenous expression of Cas9. While this model allowed us to deliver a single AAV9 expressing sgRNA targeting *SOD1* and forgoing challenges with delivering Cas9 protein, future experiments would need to deliver both Cas9 and sgRNA to have more clinical relevance. Furthermore, we used facial vein injections in neonatal P1 mice as a route of delivery. In mice, AAV delivered via facial vein injections at p1 can cross the nascent blood brain barrier and distribute to both the brain and spinal cord with comparatively high efficiency. Clinically, this route of delivery is not feasible, as adult patients have fully formed blood-brain barriers and thus would prevent distribution of vectors throughout the CNS. Additionally, we observed high rates

of indels in the liver after facial vein injections (~70%), much higher than observed in either the brain or spinal cord, a concern for patients, as that could potentially cause unforeseen adverse effects in patients.

5.2 ICV delivery of Cas9 and sgSOD1 prolongs survival in *SOD1*^{G93A} mice

Our experiments demonstrate that genome editing of *SOD1* using a dual AAV9 vector, ICV delivery scheme delays onset and prolongs survival in *SOD1*^{G93A} mice. We showed that CRISPR treatment improves motor function of mice as measurement by grip strength and rotarod performance and survival.

One caveat in interpreting the survival of the sgSOD1 mice was the lack of a control group which received Cas9 and a guide RNA that cleaved DNA at a 'safe harbor', a genomic site where gene editing would have no endogenous gene activity. Such a control group could distinguish positive effects from *SOD1* silencing from potential effects that occur after any DNA cleavage. For example, it is documented that DNA cleavage from Cas9 can activate the p53 pathway[134], which could impact motor neuron health and overall survival.

Our experiments also demonstrate successful silencing of *SOD1* gene expression, and subsequent protein reduction as measured by ELISA assays and gel capillary Western blotting. Interestingly, we observed in the spinal cord, an enhancement of gene silencing in the motor neurons. This enhancement is

likely due to the tropism of the AAV9 vector in which motor neurons where transduced at higher rates than other cell types. It is well documented that toxicity from SOD1 is not exclusively cell-autonomous, and silencing *SOD1* in glial cells and oligodendrocytes prolong survival[80,133,134]. Future strategies to delivery AAVs carrying Cas9 could employ testing a variety of AAV capsids to achieve higher survival.

We show that CRISPR treatment preserves distal axonal architecture based on measuring intact neuromuscular junctions. Denervation of the neuromuscular junction is an early onset symptom in *SOD1* transgenic mouse models and impaired neuromuscular junctions can be detected in 4-6 week old mice[128]. It is widely reported that the large diameter α-axons in the ventral root of ALS patients and *SOD1*^{G93A} mice undergo degeneration[40–42]. We observed that silencing of *SOD1* reduces degeneration of large diameter α-axons in the ventral root of *SOD1*^{G93A} mice.

We observed a level of indel formation and survival prolongation similar to that of Gaj *et al*, where a single AAV vector expressing saCas9 was injected via facial vein. Our experimental design, however differed from Gaj *et al* if a few key ways; we used spCas9 and we used a dual AAV vector approach. spCas9 is more widely-used and has a more prevalent PAM compared to saCas9, thus making it a more practical platform for which to develop gene-silencing strategies.

Our study is also distinguished by the use of TTC to measure *in vivo* net axonal transport. This new assay provides an *in vivo*, repeatable assay of neuron function. This assay documented that the benefit of *SOD1* silencing is evident as early as day 85. To our knowledge, no other trials of therapy in *SOD1* ALS have employed axonal transport as an outcome measure. Future studies using net axonal transport at even earlier timepoints are critical for understanding etiology of ALS and optimizing timing of Cas9 therapies.

In our studies we did not detect a decrease in reactive astrocytosis or microgliosis at tissue endpoint in our sgSOD1 mice when compared to controls. However, since we looked at disease endpoint, it might be possible that we did delay onset of these symptoms. Investigation of astrocytosis and microgliosis at earlier endpoints is therefore warranted.

In our studies, we use an sgRNA targeting both mutant and wildtype *SOD1*. Our sgRNA can potentially target a large number of ALS-associated *SOD1* mutations [12]. Future studies may benefit from the use of an allele-specific guide targeting only mutant *SOD1*.

5.3 Degree of indel formation and degree of SOD1 knockdown discrepancy

One interesting observation that occurred both in our studies and by Gaj *et al*, was the relatively low indel percentage (between 0.2 and 5% in the brain and spinal cord) and the relatively high protein silencing (up to 60% SOD1

knockdown detected by ELISA in the cortex). The discrepancy between the low genomic indel percentage and the high knockdown is unexpected. I speculate that the discrepancy may be explained by an inability of our deep sequencing methods to detect large-scale deletions of multiple copies of *SOD1* in the transgene cassette, and as such underreports the true amount of edited *SOD1* gene copies. The *SOD1*^{G93A} mouse that we used as a model has 25-30 copies of human *SOD1*, which is different than what occurs in patients, as the majority of *SOD1* patients have one mutant copy. It has been observed that Cas9 can induce largescale deletions when targeted to multiple sites on the same chromosome[138]. Targeting *SOD1* in transgenic mice causes multiple breaks in the chromosome and may cause large scale deletions. Such deletions would not be detected by either our deep sequencing methods or by the methods described in Gaj *et al* and would cause underrepresentation of percent of edited *SOD1* copies. Looking forward, to account for the magnitude and effect of chromosomal deletions by Cas9, future studies could employ *SOD1* knock-in models, in which only one transgenic copy of *SOD1* is present in the mouse *Sod1* locus. In this model, the rate of large-scale deletions would be less as Cas9 is no longer targeting multiple locations on the same chromosome. Additionally, any deletions observe would possibly be more relevant to what would occur in patients.

To further probe the disparity between indel editing percentage and protein knockdown percentages, we looked at SOD1 mRNA using ddPCR. Surprisingly, we saw no differences in spinal cord motor neuron SOD1 levels

between sgSOD1 mice and control mice, (i.e., non-treated and sgControl mice) (Fig. 20). Furthermore, there was no detectable difference in SOD1 mRNA levels between motor neurons and dorsal horn tissue. This could suggest that our sgSOD1 treatment does not appreciably change mRNA abundance, rather it works by limiting translation. These results, however, disagree with our *in vitro* data showing knockdown of SOD1 mRNA via qPCR. A more throughout analysis using ddPCR with multiple references is thus warranted.

5.4 Decrease in SOD1 immunopositive, high molecular weight species

It is widely accepted that misfolded and aggregate SOD1 are toxic and play a role in etiology and/or pathology of ALS. Preclinical strategies targeting toxic misfolded forms of SOD1 have increased survival in mouse models of ALS[34]. Therefore, demonstrated decrease of misfolded SOD1 may partially explain the survival benefit observed in sgSOD1 mice. In our gel capillary western blot, we noticed in all SOD1 samples the presence of immunoreactive bands sized 44 and 62 kilodaltons. Given the stability of misfolded SOD1[133], and previous histological evidence of the presence of SOD1 aggregation found in mice as young as p90[139] we speculate that these may represented non-denatured SOD1 dimer and trimers. The trimeric form of SOD1 is not found in healthy patients and is cytotoxic[37,133]. Furthermore, we found a decrease in

abundance of putative SOD1 trimeric bands in our sgSOD1 mice, suggesting that our strategy may reduce the toxic oligomeric forms of SOD1. More experimentation, however, is needed to reach definite conclusions.

One caveat to data from the gel capillary western blot data is the antibody. The antibody we used generated one singular SOD1 band at 25 kilodaltons. We expected to observe two SOD1 bands, the human band at 16 kilodaltons and a mouse with a slightly lower molecular weight. It is unclear as to why SOD1 runs at a higher apparent molecular weight in the gel capillary western blot, and why there is not two distinct human and mouse bands. It is likely that the mouse Sod1 is present and runs at the same size of human SOD1. This change in apparent weight of SOD1 may also be from ubiquitination status of SOD1. Repeating the molecular assays with increased number of mice and with different antibodies will increase our confidence in the results.

5.5 Previous *SOD1* silencing paradigms

The ICV experiments resulted in an approximate 15% increase in lifespan in *SOD1*^{G93A} mice. When benchmarking the results from the ICV experiments from other attempts to knockdown SOD1 via exogenously delivered mechanisms, comparisons can be made to design future experiments.

Foust *et al,* used the same AAV delivery vector and facial vein injections to deliver shRNA and achieved 39% increase survival. Stoica *et al* used the

same AAV vector and ICV injections to deliver miRNA targeting *SOD1* and achieved a 50% increase in survival. Borel *et al.* also used AAV vector rAAVrh10 and tail vein injections to deliver artificial miRNA and achieved a 21% increase in survival. Given that both ICV and facial veins have been used to achieve higher survival, future experiments involving sgSOD1 should consider testing various titers to achieve maximum survival.

One early concern regarding our experimental paradigm was the possibility that dual delivery of two AAV vectors would be inherently ineffective at transducing enough cells to confer a survival benefit . Since *SOD1* silencing required transduction of both AAV vectors, one carrying Cas9 and the other carrying sgSOD1, we thought it possible the odds of each cell being co-transduced could be low enough that insufficient amounts of *SOD1* silencing would occur and no improvements in survival would be observed. Our results, however, yielded similar results in both indel percentages and survival compared to Gaj *et al*, who used a single AAV experimental paradigm to delivery Cas9 and guide RNA. Similar indel percentages and survival amongst this work and work by Gaj *et al*, suggests that coincident transduction of a two AAV delivery paradigm is not a limiting factor for *SOD1* silencing.

Vector	Construct	Delivery	Median survival untreated vs treated (days)	Δ days	Author
Chemically modified siRNA		Long term infusion	125 vs 133	8	Wang…Xu 2008
AAV9	shRNA	Temporal Vein	132 vs 183.5	51.5	Foust…Kaspar 2013
AAV9	miRNA	ICV	137 vs 206	69	Stoica…Esteves 2016
rAAVrh10	miRNA	Tail Vein	131 vs 158	27	Florie…Mueller 2016
Mut AAV9	saCas9	Facial Vein	124 vs 151	27	Gaj…Schaffer 2017
AAV9	spCas9	ICV	134 vs 154	20	***

Table 5. Comparison to other SOD1 knockdown experiments

Results from our experiments in red.

5.6 Considerations for clinical applications of Cas9-mediated *SOD1* silencing

Several considerations need to be addressed before a dual vector AAV9 Cas9 strategy can be considered for clinical studies. One such consideration that need further scrutiny is the timing and route of delivery. In both studies, we administered AAVs long before onset of symptoms. From a pathologic perspective, delivery of gene therapy before onset of symptoms is desirable, as maximum benefit is correlated with earlier intervention[73]. Preclinical therapy, however, is not currently practiced for genetic disorders. Nevertheless, preclinical therapy may become feasible with early genetic screening for *SOD1* mutations.

While AAV9 is a safe viral vehicle and there are numerous clinical trials utilizing AAV9, AAVs persist in cells and presumably expressed their genetic

cargo over a long time, which increases likelihood of Cas9 off-target editing[140]. To account for this, studies utilizing methods to reduce or transiently express Cas9, such as delivering Cas9 in activatable AAVs, lipid nanoparticles or exosomes, could be employed.

Enhancing CNS tissue specificity of AAV vectors could both increase transduction of CNS tissue and reduce peripheral transduction thus, improve therapeutic potential. New AAV vectors with increased capability of crossing the blood-brain barrier and transducing brain and spinal cord tissue could potentially increase the efficiency and decrease off-tissue targeting of CRISPR delivery for ALS[109].

Another dimension to be considered for optimization was the engineering of Cas9 and nuclear localization signals. Recent work has demonstrated that nuclear localization of Cas9 correlates with editing efficiency and designing Cas9 with multiple copies of NLS increases nuclear localization[141] The Cas9 construct used in these experiments had one 3' and one 5' NLS signal. After immunostaining for Cas9 in spinal cord section, we observed that the majority of Cas9 signal was in the cytoplasm and not the nucleus (Fig. 13D). This findings are consistent with other published findings[141]. Future studies could employ a Cas9 with increased copies of NLS to boost nuclear localization.

In summary, we report that dual AAV9 delivery of spCas9 and guide RNA delays disease onset and prolongs survival in a mouse model of ALS. Our study

provides a blueprint to develop effective spCas9-based tools to study *in vivo* genome editing for ALS genes.

Bibliography

1. Mou, H., Kennedy, Z., Anderson, D. G., Yin, H. & Xue, W. Precision cancer mouse models through genome editing with CRISPR-Cas9. *Genome Med* **7**, 53 (2015).
2. Rowland, L. P. & Shneider, N. A. Amyotrophic Lateral Sclerosis. *New England Journal of Medicine* **344**, 1688–1700 (2001).
3. Hirtz, D. *et al.* How common are the "common" neurologic disorders? *Neurology* **68**, 326–337 (2007).
4. Logroscino, G. *et al.* Incidence of Amyotrophic Lateral Sclerosis in Europe. *J Neurol Neurosurg Psychiatry* **81**, 385–390 (2010).
5. Von Braunmuhl, A. Picksche Krankeit und amyotrophische Lateralsklerose. *Allg Z Psychial Psychischgerichtliche Med* **96**, 364–366 (1932).
6. Neumann, M. *et al.* A new subtype of frontotemporal lobar degeneration with FUS pathology. *Brain* **132**, 2922–2931 (2009).
7. Arai, T. *et al.* TDP-43 is a component of ubiquitin-positive tau-negative inclusions in frontotemporal lobar degeneration and amyotrophic lateral sclerosis. *Biochemical and Biophysical Research Communications* **351**, 602–611 (2006).
8. Zoccolella, S. *et al.* Riluzole and amyotrophic lateral sclerosis survival: a population-based study in southern Italy. *Eur. J. Neurol.* **14**, 262–268 (2007).
9. Abe, K. *et al.* Confirmatory double-blind, parallel-group, placebo-controlled study of efficacy and safety of edaravone (MCI-186) in amyotrophic lateral sclerosis patients.

Amyotrophic Lateral Sclerosis and Frontotemporal Degeneration **15**, 610–617 (2014).

10. Ishikawa, A. *et al.* Edaravone inhibits the expression of vascular endothelial growth factor in human astrocytes exposed to hypoxia. *Neuroscience Research* **59**, 406–412 (2007).
11. Rosen, D. R. *et al.* Mutations in Cu/Zn superoxide dismutase gene are associated with familial amyotrophic lateral sclerosis. *Nature* **362**, 59–62 (1993).
12. Abel, O., Powell, J. F., Andersen, P. M. & Al-Chalabi, A. ALSoD: A user-friendly online bioinformatics tool for amyotrophic lateral sclerosis genetics. *Hum. Mutat.* **33**, 1345–1351 (2012).
13. Rotunno, M. S. & Bosco, D. A. An emerging role for misfolded wild-type SOD1 in sporadic ALS pathogenesis. *Cellular and molecular mechanisms of motor neuron death in amyotrophic lateral sclerosis* 110 (2015).
14. Borel, F. *et al.* Therapeutic rAAVrh10 Mediated SOD1 Silencing in Adult SOD1(G93A) Mice and Nonhuman Primates. *Hum. Gene Ther.* **27**, 19–31 (2016).
15. Bosco, D. A. *et al.* Wild-type and mutant SOD1 share an aberrant conformation and a common pathogenic pathway in ALS. *Nat Neurosci* **13**, 1396–1403 (2010).
16. Bruijn, L. I. *et al.* Aggregation and Motor Neuron Toxicity of an ALS-Linked SOD1 Mutant Independent from Wild-Type SOD1. *Science* **281**, 1851–1854 (1998).
17. Melanie Leitner, Shelia Menzies & Cathleen Lutz. *Working with ALS Mice. Guidelines for preclinical testing & colony management*. (Prize4Life, 2009).

18. Pardo, C. A. *et al.* Superoxide dismutase is an abundant component in cell bodies, dendrites, and axons of motor neurons and in a subset of other neurons. *Proc Natl Acad Sci U S A* **92**, 954–958 (1995).
19. Seetharaman, S. V. *et al.* Immature Copper-Zinc Superoxide Dismutase and Familial Amyotrophic Lateral Sclerosis. *Exp Biol Med (Maywood)* **234**, 1140–1154 (2009).
20. Leal, S. S., Cardoso, I., Valentine, J. S. & Gomes, C. M. Calcium ions promote superoxide dismutase 1 (SOD1) aggregation into non-fibrillar amyloid: a link to toxic effects of calcium overload in amyotrophic lateral sclerosis (ALS)? *J. Biol. Chem.* **288**, 25219–25228 (2013).
21. Getzoff, E. D. *et al.* Faster superoxide dismutase mutants designed by enhancing electrostatic guidance. *Nature* **358**, 347 (1992).
22. Seetharaman, S. V. *et al.* Disrupted Zinc-Binding Sites in Structures of Pathogenic SOD1 Variants D124V and H80R. *Biochemistry* **49**, 5714–5725 (2010).
23. Wang, H. *et al.* Therapeutic Gene Silencing Delivered by a Chemically Modified Small Interfering RNA against Mutant SOD1 Slows Amyotrophic Lateral Sclerosis Progression. *J. Biol. Chem.* **283**, 15845–15852 (2008).
24. Islam, M. T. Oxidative stress and mitochondrial dysfunction-linked neurodegenerative disorders. *Neurological Research* **39**, 73–82 (2017).
25. Bonafede, R. & Mariotti, R. ALS Pathogenesis and Therapeutic Approaches: The Role of Mesenchymal Stem Cells and Extracellular Vesicles. *Front Cell Neurosci* **11**, 80 (2017).

26. Hayward, L. J. *et al.* Decreased Metallation and Activity in Subsets of Mutant Superoxide Dismutases Associated with Familial Amyotrophic Lateral Sclerosis ,. *J. Biol. Chem.* **277**, 15923–15931 (2002).
27. Reaume, A. G. *et al.* Motor neurons in Cu/Zn superoxide dismutase-deficient mice develop normally but exhibit enhanced cell death after axonal injury. *Nat. Genet.* **13**, 43–47 (1996).
28. Sau, D. *et al.* Mutation of SOD1 in ALS: a gain of a loss of function. *Hum Mol Genet* **16**, 1604–1618 (2007).
29. Saccon, R. A., Bunton-Stasyshyn, R. K. A., Fisher, E. M. C. & Fratta, P. Is SOD1 loss of function involved in amyotrophic lateral sclerosis? *Brain* awt097 (2013). doi:10.1093/brain/awt097
30. Forsberg, K. *et al.* Misfolded SOD1 inclusions in patients with mutations in C9orf72 and other ALS/FTD-associated genes. *J. Neurol. Neurosurg. Psychiatry* (2019). doi:10.1136/jnnp-2018-319386
31. Durham, H. D., Roy, J., Dong, L. & Figlewicz, D. A. Aggregation of Mutant Cu/Zn Superoxide Dismutase Proteins in a Culture Model of ALS. *J Neuropathol Exp Neurol* **56**, 523–530 (1997).
32. Grad, L. I. *et al.* Intercellular propagated misfolding of wild-type Cu/Zn superoxide dismutase occurs via exosome-dependent and -independent mechanisms. *Proc Natl Acad Sci U S A* **111**, 3620–3625 (2014).

33. Münch, C., O'Brien, J. & Bertolotti, A. Prion-like propagation of mutant superoxide dismutase-1 misfolding in neuronal cells. *Proc. Natl. Acad. Sci. U.S.A.* **108**, 3548–3553 (2011).
34. Gros-Louis, F., Soucy, G., Larivière, R. & Julien, J.-P. Intracerebroventricular infusion of monoclonal antibody or its derived Fab fragment against misfolded forms of SOD1 mutant delays mortality in a mouse model of ALS. *Journal of Neurochemistry* **113**, 1188–1199 (2010).
35. Brotherton, T. E. *et al.* Localization of a toxic form of superoxide dismutase 1 protein to pathologically affected tissues in familial ALS. *PNAS* **109**, 5505–5510 (2012).
36. Johnston, J. A., Dalton, M. J., Gurney, M. E. & Kopito, R. R. Formation of high molecular weight complexes of mutant Cu,Zn-superoxide dismutase in a mouse model for familial amyotrophic lateral sclerosis. *Proc Natl Acad Sci U S A* **97**, 12571–12576 (2000).
37. Zhu, C., Beck, M. V., Griffith, J. D., Deshmukh, M. & Dokholyan, N. V. Large SOD1 aggregates, unlike trimeric SOD1, do not impact cell viability in a model of amyotrophic lateral sclerosis. *PNAS* **115**, 4661–4665 (2018).
38. Sundaramoorthy, V. *et al.* Extracellular wildtype and mutant SOD1 induces ER-Golgi pathology characteristic of amyotrophic lateral sclerosis in neuronal cells. *Cell. Mol. Life Sci.* **70**, 4181–4195 (2013).
39. Cutler, R. G., Pedersen, W. A., Camandola, S., Rothstein, J. D. & Mattson, M. P. Evidence that accumulation of ceramides and cholesterol esters mediates oxidative

stress–induced death of motor neurons in amyotrophic lateral sclerosis. *Annals of Neurology* **52**, 448–457 (2002).

40. Barber, S. C. & Shaw, P. J. Oxidative stress in ALS: key role in motor neuron injury and therapeutic target. *Free Radic. Biol. Med.* **48**, 629–641 (2010).
41. Eisen, A. Clinical Electrophysiology of the Upper and Lower Motor Neuron in Amyotrophic Lateral Sclerosis. *Seminars in Neurology* **21**, 141–154 (2001).
42. de Carvalho, M., Eisen, A., Krieger, C. & Swash, M. Motoneuron firing in amyotrophic lateral sclerosis (ALS). *Front Hum Neurosci* **8**, (2014).
43. Shaw, P. J., Forrest, V., Ince, P. G., Richardson, J. P. & Wastell, H. J. CSF and Plasma Amino Acid Levels in Motor Neuron Disease: Elevation of CSF Glutamate in a Subset of Patients. *Neurodegeneration* **4**, 209–216 (1995).
44. Spreux-Varoquaux, O. *et al.* Glutamate levels in cerebrospinal fluid in amyotrophic lateral sclerosis: a reappraisal using a new HPLC method with coulometric detection in a large cohort of patients. *Journal of the Neurological Sciences* **193**, 73–78 (2002).
45. Lin, C.-L. G. *et al.* Aberrant RNA Processing in a Neurodegenerative Disease: the Cause for Absent EAAT2, a Glutamate Transporter, in Amyotrophic Lateral Sclerosis. *Neuron* **20**, 589–602 (1998).
46. Fray, A. E. *et al.* The expression of the glial glutamate transporter protein EAAT2 in motor neuron disease: an immunohistochemical study. *European Journal of Neuroscience* **10**, 2481–2489 (1998).

47. Rothstein, J. D., Kammen, M. V., Levey, A. I., Martin, L. J. & Kuncl, R. W. Selective loss of glial glutamate transporter GLT-1 in amyotrophic lateral sclerosis. *Annals of Neurology* **38**, 73–84 (1995).
48. von Lewinski, F. & Keller, B. U. Ca2+, mitochondria and selective motorneuron vulnerability: implications for ALS. *TRENDS in Neuroscience* **28**, 494–500 (2005).
49. Trotti, D., Danbolt, N. C. & Volterra, A. Glutamate transporters are oxidant-vulnerable: a molecular link between oxidative and excitotoxic neurodegeneration? *Trends in Pharmacological Sciences* **19**, 328–334 (1998).
50. Van Den Bosch, L., Van Damme, P., Bogaert, E. & Robberecht, W. The role of excitotoxicity in the pathogenesis of amyotrophic lateral sclerosis. *Biochimica et Biophysica Acta (BBA) - Molecular Basis of Disease* **1762**, 1068–1082 (2006).
51. Grosskreutz, J., Van Den Bosch, L. & Keller, B. U. Calcium dysregulation in amyotrophic lateral sclerosis. *Cell Calcium* **47**, 165–174 (2010).
52. Tan, W., Pasinelli, P. & Trotti, D. Role of mitochondria in mutant SOD1 linked amyotrophic lateral sclerosis. *Biochim Biophys Acta* **1842**, 1295–1301 (2014).
53. Hirano, A. *et al.* Fine Structural Study of Neurofibrillary Changes in a Family with Amyotrophic Lateral Sclerosis. *J Neuropathol Exp Neurol* **43**, 471–480 (1984).
54. Pramanik, K. C., Boreddy, S. R. & Srivastava, S. K. Role of Mitochondrial Electron Transport Chain Complexes in Capsaicin Mediated Oxidative Stress Leading to Apoptosis in Pancreatic Cancer Cells. *PLoS One* **6**, (2011).
55. Rasola, A. & Bernardi, P. The mitochondrial permeability transition pore and its involvement in cell death and in disease pathogenesis. *Apoptosis* **12**, 815–833 (2007).

56. Contreras, L., Drago, I., Zampese, E. & Pozzan, T. Mitochondria: The calcium connection. *Biochimica et Biophysica Acta (BBA) - Bioenergetics* **1797**, 607–618 (2010).

57. Galluzzi, L., Blomgren, K. & Kroemer, G. Mitochondrial membrane permeabilization in neuronal injury. *Nat. Rev. Neurosci.* **10**, 481–494 (2009).

58. Pedrini, S. *et al.* ALS-linked mutant SOD1 damages mitochondria by promoting conformational changes in Bcl-2. *Hum Mol Genet* **19**, 2974–2986 (2010).

59. Pasinelli, P. *et al.* Amyotrophic Lateral Sclerosis-Associated SOD1 Mutant Proteins Bind and Aggregate with Bcl-2 in Spinal Cord Mitochondria. *Neuron* **43**, 19–30 (2004).

60. Kabuta, T., Suzuki, Y. & Wada, K. Degradation of Amyotrophic Lateral Sclerosis-linked Mutant Cu,Zn-Superoxide Dismutase Proteins by Macroautophagy and the Proteasome. *J. Biol. Chem.* **281**, 30524–30533 (2006).

61. Yonashiro, R. *et al.* Mitochondrial Ubiquitin Ligase MITOL Ubiquitinates Mutant SOD1 and Attenuates Mutant SOD1-induced Reactive Oxygen Species Generation. *MBoC* **20**, 4524–4530 (2009).

62. Urushitani, M. *et al.* CHIP promotes proteasomal degradation of familial ALS-linked mutant SOD1 by ubiquitinating Hsp/Hsc70. *Journal of Neurochemistry* **90**, 231–244 (2004).

63. Miyazaki, K. *et al.* NEDL1, a Novel Ubiquitin-protein Isopeptide Ligase for Dishevelled-1, Targets Mutant Superoxide Dismutase-1. *J. Biol. Chem.* **279**, 11327–11335 (2004).

64. Hishikawa, N. *et al.* Dorfin Localizes to the Ubiquitylated Inclusions in Parkinson's Disease, Dementia with Lewy Bodies, Multiple System Atrophy, and Amyotrophic Lateral Sclerosis. *Am J Pathol* **163**, 609–619 (2003).
65. Shi, Y. *et al.* Identification of CHIP as a novel causative gene for autosomal recessive cerebellar ataxia. *PLoS ONE* **8**, e81884 (2013).
66. Mendonça, D. M. F., Chimelli, L. & Martinez, A. M. B. Expression of ubiquitin and proteasome in motorneurons and astrocytes of spinal cords from patients with amyotrophic lateral sclerosis. *Neuroscience Letters* **404**, 315–319 (2006).
67. Pattingre, S. *et al.* Bcl-2 Antiapoptotic Proteins Inhibit Beclin 1-Dependent Autophagy. *Cell* **122**, 927–939 (2005).
68. Li, L., Zhang, X. & Le, W. Altered macroautophagy in the spinal cord of SOD1 mutant mice. *Autophagy* **4**, 290–293 (2008).
69. Gal, J. *et al.* Sequestosome 1/p62 links familial ALS mutant SOD1 to LC3 via an ubiquitin-independent mechanism. *Journal of Neurochemistry* **111**, 1062–1073 (2009).
70. Teyssou, E. *et al.* Mutations in SQSTM1 encoding p62 in amyotrophic lateral sclerosis: genetics and neuropathology. *Acta Neuropathol.* **125**, 511–522 (2013).
71. Imamura, K. *et al.* The Src/c-Abl pathway is a potential therapeutic target in amyotrophic lateral sclerosis. *Science Translational Medicine* **9**, eaaf3962 (2017).
72. Stoica, L. *et al.* Adeno-associated virus–delivered artificial microRNA extends survival and delays paralysis in an amyotrophic lateral sclerosis mouse model. *Ann Neurol.* **79**, 687–700 (2016).

73. Foust, K. D. *et al.* Therapeutic AAV9-mediated Suppression of Mutant SOD1 Slows Disease Progression and Extends Survival in Models of Inherited ALS. *Mol Ther* **21**, 2148–2159 (2013).

74. Thomsen, G. M. *et al.* Delayed Disease Onset and Extended Survival in the SOD1G93A Rat Model of Amyotrophic Lateral Sclerosis after Suppression of Mutant SOD1 in the Motor Cortex. *J. Neurosci.* **34**, 15587–15600 (2014).

75. JCI - Antisense oligonucleotide therapy for neurodegenerative disease. Available at: https://www.jci.org/articles/view/25424. (Accessed: 3rd August 2018)

76. Wang, H. *et al.* Widespread spinal cord transduction by intrathecal injection of rAAV delivers efficacious RNAi therapy for amyotrophic lateral sclerosis. *Hum Mol Genet* **23**, 668–681 (2014).

77. Ralph, G. S. *et al.* Silencing mutant SOD1 using RNAi protects against neurodegeneration and extends survival in an ALS model. *Nat Med* **11**, 429–433 (2005).

78. Saito, Y. *et al.* Transgenic Small Interfering RNA Halts Amyotrophic Lateral Sclerosis in a Mouse Model. *J. Biol. Chem.* **280**, 42826–42830 (2005).

79. Zhang, Y. *et al.* Liver specific expression of Cu/ZnSOD extends the lifespan of Sod1 null mice. *Mechanisms of Ageing and Development* **154**, 1–8 (2016).

80. Zhao, W. *et al.* Extracellular mutant SOD1 induces microglial-mediated motoneuron injury. *Glia* **58**, 231–243 (2010).

81. Nagai, M. *et al.* Astrocytes expressing ALS-linked mutated SOD1 release factors selectively toxic to motor neurons. *Nat Neurosci* **10**, 615–622 (2007).

82. Ferraiuolo, L. *et al.* Oligodendrocytes contribute to motor neuron death in ALS via SOD1-dependent mechanism. *PNAS* **113**, E6496–E6505 (2016).

83. Wong, M. & Martin, L. J. Skeletal muscle-restricted expression of human SOD1 causes motor neuron degeneration in transgenic mice. *Hum Mol Genet* **19**, 2284–2302 (2010).

84. Dirren, E. *et al.* SOD1 silencing in motoneurons or glia rescues neuromuscular function in ALS mice. *Ann Clin Transl Neurol* **2**, 167–184 (2015).

85. Miller, T. M. *et al.* Gene transfer demonstrates that muscle is not a primary target for non-cell-autonomous toxicity in familial amyotrophic lateral sclerosis. *Proc. Natl. Acad. Sci. U.S.A.* **103**, 19546–19551 (2006).

86. Towne, C., Setola, V., Schneider, B. L. & Aebischer, P. Neuroprotection by gene therapy targeting mutant SOD1 in individual pools of motor neurons does not translate into therapeutic benefit in fALS mice. *Mol. Ther.* **19**, 274–283 (2011).

87. Towne, C., Raoul, C., Schneider, B. L. & Aebischer, P. Systemic AAV6 Delivery Mediating RNA Interference Against SOD1: Neuromuscular Transduction Does Not Alter Disease Progression in fALS Mice. *Molecular Therapy* **16**, 1018–1025 (2008).

88. Özdinler, P. H. *et al.* Corticospinal Motor Neurons and Related Subcerebral Projection Neurons Undergo Early and Specific Neurodegeneration in hSOD1G93A Transgenic ALS Mice. *J. Neurosci.* **31**, 4166–4177 (2011).

89. Mojica, F. J., Díez-Villaseñor, C., Soria, E. & Juez, G. Biological significance of a family of regularly spaced repeats in the genomes of Archaea, Bacteria and mitochondria. *Mol. Microbiol.* **36**, 244–246 (2000).

90. Koonin, E. V., Makarova, K. S. & Zhang, F. Diversity, classification and evolution of CRISPR-Cas systems. *Curr. Opin. Microbiol.* **37**, 67–78 (2017).
91. Marraffini, L. A. & Sontheimer, E. J. CRISPR Interference Limits Horizontal Gene Transfer in Staphylococci by Targeting DNA. *Science* **322**, 1843–1845 (2008).
92. Adli, M. The CRISPR tool kit for genome editing and beyond. *Nat Commun* **9**, 1–13 (2018).
93. Jinek, M. *et al.* A Programmable Dual-RNA–Guided DNA Endonuclease in Adaptive Bacterial Immunity. *Science* **337**, 816–821 (2012).
94. Jinek, M. *et al.* Structures of Cas9 Endonucleases Reveal RNA-Mediated Conformational Activation. *Science* **343**, 1247997 (2014).
95. Anders, C., Niewoehner, O., Duerst, A. & Jinek, M. Structural basis of PAM-dependent target DNA recognition by the Cas9 endonuclease. *Nature* **513**, 569–573 (2014).
96. Swiech, L. *et al.* In vivo interrogation of gene function in the mammalian brain using CRISPR-Cas9. *Nat Biotech* **33**, 102–106 (2015).
97. Gaj, T. *et al.* In vivo genome editing improves motor function and extends survival in a mouse model of ALS. *Science Advances* **3**, eaar3952 (2017).
98. Xie, Q. *et al.* The atomic structure of adeno-associated virus (AAV-2), a vector for human gene therapy. *PNAS* **99**, 10405–10410 (2002).
99. Byrnes, A. *Summary Basis for Regulatory Action*. 15 (FDA, 2019).

100. Vandamme, C., Adjali, O. & Mingozzi, F. Unraveling the Complex Story of Immune Responses to AAV Vectors Trial After Trial. *Hum Gene Ther* **28**, 1061–1074 (2017).

101. Gao, G., Vandenberghe, L. H. & Wilson, J. M. New Recombinant Serotypes of AAV Vectors. (2005). doi:info:doi/10.2174/1566523054065057

102. Hastie, E. & Samulski, R. J. Adeno-Associated Virus at 50: A Golden Anniversary of Discovery, Research, and Gene Therapy Success—A Personal Perspective. *Human Gene Therapy* **26**, 257–265 (2015).

103. Straus, S. E., Sebring, E. D. & Rose, J. A. Concatemers of alternating plus and minus strands are intermediates in adenovirus-associated virus DNA synthesis. *PNAS* **73**, 742–746 (1976).

104. Pillay, S. *et al.* An essential receptor for adeno-associated virus infection. *Nature* **530**, 108–112 (2016).

105. Dudek, A. M. *et al.* An Alternate Route for Adeno-associated Virus (AAV) Entry Independent of AAV Receptor. *J. Virol.* **92**, (2018).

106. Li, C. *et al.* Adeno-associated virus capsid antigen presentation is dependent on endosomal escape. *J Clin Invest* **123**, 1390–1401 (2013).

107. Nicolson, S. C. & Samulski, R. J. Recombinant Adeno-Associated Virus Utilizes Host Cell Nuclear Import Machinery To Enter the Nucleus. *Journal of Virology* **88**, 4132–4144 (2014).

108. Yin, H. *et al.* Partial DNA-guided Cas9 enables genome editing with reduced off-target activity. *Nature Chemical Biology* **14**, 311–316 (2018).

109. Zhang, H. *et al.* Several rAAV Vectors Efficiently Cross the Blood–brain Barrier and Transduce Neurons and Astrocytes in the Neonatal Mouse Central Nervous System. *Mol Ther* **19**, 1440–1448 (2011).

110. Deverman, B. E. *et al.* Cre-dependent selection yields AAV variants for widespread gene transfer to the adult brain. *Nat. Biotechnol.* **34**, 204–209 (2016).

111. McCarty, D. M., Monahan, P. E. & Samulski, R. J. Self-complementary recombinant adeno-associated virus (scAAV) vectors promote efficient transduction independently of DNA synthesis. *Gene Therapy* **8**, 1248 (2001).

112. Wu, T. *et al.* Self-complementary AAVs Induce More Potent Transgene Product-specific Immune Responses Compared to a Single-stranded Genome. *Molecular Therapy* **20**, 572–579 (2012).

113. Boutin, S. *et al.* Prevalence of Serum IgG and Neutralizing Factors Against Adeno-Associated Virus (AAV) Types 1, 2, 5, 6, 8, and 9 in the Healthy Population: Implications for Gene Therapy Using AAV Vectors. *Human Gene Therapy* **21**, 704–712 (2010).

114. Mingozzi, F. *et al.* $CD8^+$ T-cell responses to adeno-associated virus capsid in humans. *Nature Medicine* **13**, 419–422 (2007).

115. Calcedo, R., Vandenberghe, L. H., Gao, G., Lin, J. & Wilson, J. M. Worldwide Epidemiology of Neutralizing Antibodies to Adeno-Associated Viruses. *J Infect Dis* **199**, 381–390 (2009).

116. Gombash Lampe, S. E., Kaspar, B. K. & Foust, K. D. Intravenous Injections in Neonatal Mice. *Journal of Visualized Experiments* (2014). doi:10.3791/52037

117. Clement, K. *et al.* CRISPResso2 provides accurate and rapid genome editing sequence analysis. *Nat. Biotechnol.* **37**, 224–226 (2019).

118. Benn, S. C. *et al.* Tetanus toxin fragment C fusion facilitates protein delivery to CNS neurons from cerebrospinal fluid in mice. *Journal of Neurochemistry* **95**, 1118–1131 (2005).

119. Kayatekin, C., Zitzewitz, J. A. & Matthews, C. R. Disulfide-Reduced ALS Variants of Cu, Zn Superoxide Dismutase Exhibit Increased Populations of Unfolded Species. *Journal of Molecular Biology* **398**, 320–331 (2010).

120. Zhang, J., Sun, X., Qian, Y., LaDuca, J. P. & Maquat, L. E. At least one intron is required for the nonsense-mediated decay of triosephosphate isomerase mRNA: a possible link between nuclear splicing and cytoplasmic translation. *Mol. Cell. Biol.* **18**, 5272–5283 (1998).

121. Shaw, P. J. Motor neurone disease. *BMJ* **318**, 1118–1121 (1999).

122. Taylor, J. P., Brown Jr, R. H. & Cleveland, D. W. Decoding ALS: from genes to mechanism. *Nature* **539**, 197–206 (2016).

123. Maragakis NJ & Rothstein JD. GLutamate transporters in neurologic disease. *Arch Neurol* **58**, 365–370 (2001).

124. Deng, H.-X. *et al.* Conversion to the amyotrophic lateral sclerosis phenotype is associated with intermolecular linked insoluble aggregates of SOD1 in mitochondria. *PNAS* **103**, 7142–7147 (2006).

125. Pickles, S. *et al.* Mitochondrial damage revealed by immunoselection for ALS-linked misfolded SOD1. *Hum. Mol. Genet.* ddt249 (2013). doi:10.1093/hmg/ddt249

126. Kim, S. H. *et al.* Potentiation of Amyotrophic Lateral Sclerosis (ALS)-associated TDP-43 Aggregation by the Proteasome-targeting Factor, Ubiquilin 1. *J. Biol. Chem.* **284**, 8083–8092 (2009).

127. In vivo genome editing improves motor function and extends survival in a mouse model of ALS | Science Advances. Available at: http://advances.sciencemag.org/content/3/12/eaar3952. (Accessed: 6th June 2018)

128. Rocha, M. C., Pousinha, P. A., Correia, A. M., Sebastião, A. M. & Ribeiro, J. A. Early Changes of Neuromuscular Transmission in the SOD1(G93A) Mice Model of ALS Start Long before Motor Symptoms Onset. *PLOS ONE* **8**, e73846 (2013).

129. Moloney, E. B., de Winter, F. & Verhaagen, J. ALS as a distal axonopathy: molecular mechanisms affecting neuromuscular junction stability in the presymptomatic stages of the disease. *Front. Neurosci.* **8**, (2014).

130. Fischer, L. R. *et al.* Amyotrophic lateral sclerosis is a distal axonopathy: evidence in mice and man. *Experimental Neurology* **185**, 232–240 (2004).

131. Lalancette-Hebert, M., Sharma, A., Lyashchenko, A. K. & Shneider, N. A. Gamma motor neurons survive and exacerbate alpha motor neuron degeneration in ALS. *Proc Natl Acad Sci USA* **113**, E8316–E8325 (2016).

132. Pellizzari, R., Rossetto, O., Schiavo, G. & Montecucco, C. Tetanus and botulinum neurotoxins: mechanism of action and therapeutic uses. *Philos Trans R Soc Lond B Biol Sci* **354**, 259–268 (1999).

133. Proctor, E. A. *et al.* Nonnative SOD1 trimer is toxic to motor neurons in a model of amyotrophic lateral sclerosis. *PNAS* **113**, 614–619 (2016).

134. Haapaniemi, E., Botla, S., Persson, J., Schmierer, B. & Taipale, J. CRISPR–Cas9 genome editing induces a p53-mediated DNA damage response. *Nat Med* **24**, 927–930 (2018).

137. Nguyen, M. D., Larivière, R. C. & Julien, J.-P. Reduction of axonal caliber does not alleviate motor neuron disease caused by mutant superoxide dismutase 1. *PNAS* **97**, 12306–12311 (2000).

138. Kosicki, M., Tomberg, K. & Bradley, A. Repair of double-strand breaks induced by CRISPR-Cas9 leads to large deletions and complex rearrangements. *Nat. Biotechnol.* (2018). doi:10.1038/nbt.4192

139. Stieber, A., Gonatas, J. O. & Gonatas, N. K. Aggregation of ubiquitin and a mutant ALS-linked SOD1 protein correlate with disease progression and fragmentation of the Golgi apparatus. *Journal of the Neurological Sciences* **173**, 53–62 (2000).

140. Ma, H. *et al.* CRISPR-Cas9 nuclear dynamics and target recognition in living cells. *J Cell Biol* **214**, 529–537 (2016).

141. Staahl, B. T. *et al.* Efficient genome editing in the mouse brain by local delivery of engineered Cas9 ribonucleoprotein complexes. *Nature Biotechnology* **35**, 431–434 (2017).